U.S. Department of Transportation

Federal Railroad Administration

Office of Research,
Development and Technology
Washington, DC 20590

Characterizing TC128 Steel Plasticity for Finite Element Modeling

DOT/FRA/ORD-26/14

Final Report | August 2026

REPORT DOCUMENTATION PAGE

Form Approved
OMB No. 0704-0188

1. REPORT DATE *(DD-MM-YYYY)*	**2. REPORT TYPE**	**3. DATES COVERED** *(From - To)*
19 Aug. 2026	Technical Report	May 2019 – May 2025

4. TITLE AND SUBTITLE

Characterizing TC128 Steel Plasticity for Finite Element Modeling

5a. CONTRACT NUMBER
693JJ620N000049

5b. GRANT NUMBER

5c. PROGRAM ELEMENT NUMBER

6. AUTHOR(S)

Michael Carolan: ORCID #0000-0002-8758-5739

Shaun Eshraghi: ORCID #0000-0002-8152-0838

5d. PROJECT NUMBER
51RR28A520

5e. TASK NUMBER

5f. WORK UNIT NUMBER

7. PERFORMING ORGANIZATION NAME(S) AND ADDRESS(ES)
Volpe National Transportation Systems Center
220 Binney Street
Cambridge, MA 02142

8. PERFORMING ORGANIZATION REPORT NUMBER

9. SPONSORING/MONITORING AGENCY NAME(S) AND ADDRESS(ES)
U.S. Department of Transportation
Federal Railroad Administration
1200 New Jersey Avenue, SE
Washington, DC 20590

10. SPONSOR/MONITOR'S ACRONYM(S)

11. SPONSOR/MONITOR'S REPORT NUMBER(S)
DOT/FRA/ORD-26/14

12. DISTRIBUTION/AVAILABILITY STATEMENT
This document is available to the public through the FRA website.

13. SUPPLEMENTARY NOTES
COR: Brian Won

14. ABSTRACT
The Federal Railroad Administration, through a research program to improve transportation safety for tank cars, sponsored the Volpe National Transportation Systems Center to develop and compare techniques to simulate the plastic stress-strain behavior of Association of American Railroads' TC128, Grade B (TC128) steel [1]. TC128 steel is used in the construction of tank cars designed to carry hazardous materials. This research took place between 2019 and 2025.

15. SUBJECT TERMS
Finite element analysis, tank car performance, transportation safety, hazardous materials, rolling stock, side impact test, TC128

16. SECURITY CLASSIFICATION OF:			**17. LIMITATION OF ABSTRACT**	**18. NUMBER OF PAGES**	**19a. NAME OF RESPONSIBLE PERSON**
a. REPORT	**b. ABSTRACT**	**c. THIS PAGE**		40	**19b. TELEPHONE NUMBER** *(Include area code)*

Standard Form 298 (Rev. 8/98)
Prescribed by ANSI Std. Z39.18

Acknowledgments

The regression equations for estimating the stress-strain responses described in Section 3 and Appendix A of this report were developed by former Volpe Center employee Josh Leung.

The authors acknowledge Transportation Technology Center, Inc. (now MxV Rail) and ENSCO, Inc. for performing the shell impact tests and contracting test labs for tensile testing. Tests 6, 7, 8, 9, and 11 were performed by TTCI/MxV Rail, and Test 14 was performed by Ensco. Westmoreland Mechanical Testing & Research performed tensile characterization of the TC128 steel from the tank cars in Tests 6, 7, 8, 9, and 14. For Test 11, the manufacturer of the outer tank of the tank car provided the tensile test data used in this report.

The report cover photograph is of post-impact TC128 specimens taken from the Test 11 test article. The post-impact testing and photography of the test specimens were both performed by Rocky Mountain Engineering and Materials Technology, Inc.

Contents

Illustrations

Tables

Executive Summary

The Federal Railroad Administration (FRA), through a research program to improve transportation safety for tank cars, sponsored the Volpe National Transportation Systems Center (Volpe Center) to develop and compare techniques to simulate the plastic stress-strain behavior of Association of American Railroads' (AAR) TC128, Grade B (TC128) steel [1]. TC128 steel is used in the construction of tank cars primarily designed to carry hazardous materials. This research took place between 2019 and 2025.

The test results and analyses presented in this report are part of a large research program to develop performance-based testing requirements to evaluate the crashworthiness and structural integrity of tank car designs under a shell (i.e., side) impact scenario. Transportation Technology Center, Inc. (TTCI, now MxV Rail), Ensco, and the Volpe Center collaborated to conduct shell impact tests of tank car designs and to analyze the results. Ensco or TTCI/MxV conducted the shell impact tests. The Volpe Center team performed both pre-test and post-test finite element (FE) analyses of the impact response to evaluate and improve modeling techniques for tank car puncture involving fluid-structure interaction and material failure.

For each shell impact test, one or more material testing labs conducted tensile testing on samples from the shell of the tested tank car. The team used the tensile test results to develop material inputs needed to model material failure in the full-scale FE analysis of the shell impact test. Generally, the tested tank cars were fabricated from TC128 steel, but other materials were authorized for construction (e.g., carbon steel or stainless steel, depending on the tank car specification and commodity). The methodologies described in this report for calibrating the true stress (σ_t) versus true plastic strain responses (ε^{pl}) of TC128 from limited test data are intended to support future analyses of tank cars to improve their puncture resistance. The σ_t versus ε^{pl} calibration procedures can use tensile test data from either rectangular dogbone (DB) or smooth round bar (SRB) specimen geometries to create the material model in the format required by the FE software.

This report presents two approaches to calibrating a σ_t versus ε^{pl} response. One method of calibration was an iterative approach that required the full range of stress-strain measurements from a tensile test; researchers found that this approach produced very good agreement with the tensile measurements. A second, "regression" method was developed to estimate the plastic stress-strain response of TC128 steel using limited data from a tensile test.[1] The limited data does not include stress-strain measurements over the entire tensile test. This methodology was developed because test labs typically do not record stress-strain measurements up to break of the tensile coupon, and most of the publicly available tensile data for TC128 would be categorized as limited. Additionally, researchers found that the regression method based on limited data produced a stress-strain response that was in close agreement with calibrations that used the full stress-strain test data.

[1] "Limited" data refers to only a summary that includes values for the yield strength (YS), ultimate tensile strength (UTS), and elongation at break (EB_{2in} for a 2-inch gauge length specimen, or EB_{8in} for an 8-inch gauge length specimen, as appropriate).

1. Introduction

The Federal Railroad Administration (FRA) sponsored Volpe National Transportation Systems Center (Volpe Center) to conduct research to improve plasticity modeling of Association of American Railroads' (AAR) TC128, Grade B steel [1]. Volpe Center conducted the research between 2019 and 2025. The report contains a summary of material properties on TC128 from four tank cars using standardized tensile geometries. Two methodologies are described to use the measured tensile properties to create material inputs necessary to model steel plasticity in finite element (FE) analysis. This report is a companion to a previously published report documenting the development of material fracture parameters for TC128 steel [2].

1.1 Background

In the past two decades, significant research has been conducted to analyze and improve the impact behavior and puncture resistance of railroad tank cars used to transport hazardous materials. Ultimately, government regulatory agencies in the United States (FRA and Pipeline and Hazardous Materials Safety Administration (PHMSA)) and Canada (Transport Canada (TC)) can use the results of this research program to establish performance-based requirements and to develop methods to evaluate the crashworthiness and structural integrity of different tank car designs when subjected to a standardized, repeatable shell impact scenario, such as a side impact. (see Figure 1).

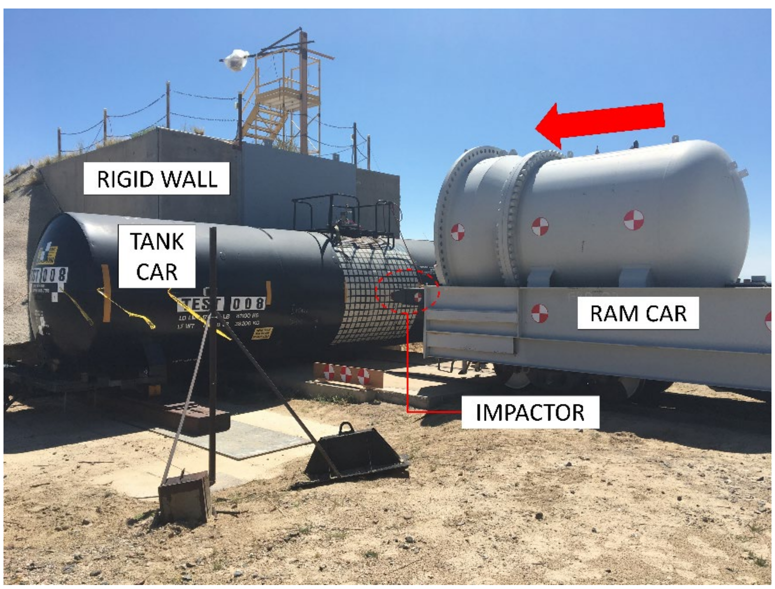

Figure 1. Standardized Shell Impact Scenario

Table 1 summarizes the tank car shell impact tests conducted since 2007. These shell impact tests involved testing tank cars constructed to various specifications and included a mix of cars designed to carry liquefied compressed gases (DOT-105), flammable liquids (DOT-111 and DOT-117), and cryogenic liquids (DOT-113). Some of these tests were performed as part of a government-industry collaborative program referred to as the Next Generation Railroad Tank Car Project (denoted in the table with †). Additional details on each test may be found in the respective test's report, as noted in the table. Tests 1 – 10 were compared and summarized in a separate report [3]. Tests denoted with a †† symbol used a tank car that was not made from

TC128 steel. Researchers selected Tests 11 and 14 for this study because they used modern TC128 tank cars and had reliable tensile data; other tests could be included in future work. The full set of shell impact tests are included for thoroughness but are not discussed further in this report.

Table 1. Summary of Tank Car Shell Impact Tests

Test *No.*	Test Date *MM/DD/YYYY*	Specification	Impact Speed *mph*	Impactor Size *inches*	Reference
1	4/26/2007	DOT-105†	14.0	17 x 23	[4]
2	7/11/2007	DOT-105†	15.1	6 x 6	[4]
3	5/18/2011	DOT-105 (w/ panel)	17.8	12 x 12	[5]
4	5/18/2013	DOT-111††	14.0	12 x 12	[6]
5	2/26/2014	DOT-112	14.7	12 x 12	[7]
6	4/27/2016	DOT-105	15.2	12 x 12	[8]
7	9/28/2016	DOT-117	13.9	12 x 12	[9]
8	8/1/2018	DOT-105	9.7	6 x 6	[10]
9	10/30/2018	DOT-111 (CPC-1232)	13.9	12 x 12	[11]
10	11/19/2019	DOT-113††	16.7	12 x 12	[12]
11	6/11/2020	DOT-113 Surrogate	17.3	12 x 12	[13]
12	7/24/2021	DOT-113 Surrogate	18.3	12 x 12	[14]
13	5/14/2022	DOT-113C120W9	22.1	12 x 12	[15]
14	3/6/2024	DOT-105	15.5	12 x 12	[16]

Figure 2 shows a still frame, taken just prior to puncture, from a high-speed camera during a 2018 test of a DOT-105 tank car (see Test 8 in Table 1). To make the test repeatable, controllable, and safe, the tank car was removed from its trucks (i.e., bogies) and placed on two skids that limit the roll of the tank car. The tank car was centered perpendicularly on a set of railroad tracks against a stiff impact wall. A ram car weighing approximately 297,000 pounds was equipped with an impact head which can vary in size and accelerated by gravity along track with a slight descending grade resulting in a controllable initial kinetic energy.

Figure 2. Still Frame from Shell Impact Test in 2018 of DOT-105 Tank Car (Test 8)

The value of a test can be increased by targeting an impact speed that is very close to the threshold speed between where the tank car does and does not puncture for a given impactor shape, size, and mass. If the tested impact speed is close to this threshold speed, regardless of whether the tank punctures, the data that is collected can be extremely valuable for quantifying the energy-absorption capacity of the tank car for the tested outage and pressure. As the test speed moves further from the center of the puncture threshold range, the value of the test data decreases.

The research team used FE analysis to model the shell impact tests and determine the target impact speed prior to each test. Similar FE analysis has been conducted to examine the puncture behavior of the railroad tank car under the generalized shell impact scenario for all the tests in Table 1. Once the FE model is validated by accurately describing the response of the tank car to the tested impact condition, other studies can be conducted using the same model to investigate different impact conditions. These additional studies can be useful for understanding the puncture resistance of the tank car in accident conditions and developing performance requirements in future rulemakings.

This report focuses on the material behavior of TC128 steel, which is widely used in the construction of tank cars used to transport hazardous materials. Specifically, this report examines several approaches to calibrating the plastic portion of the σ_t versus ε^{pl} behavior of TC128 steel for input to puncture simulations using measurements from tensile tests.

While it is a conservative engineering practice to assume minimum material properties when making design calculations, a tank car with a shell made from TC128 that only barely meets the minimum mechanical properties (see Table 2) may have a much lower ability to resist puncture than a tank car with "as-built" modern TC128 or TC128 that greatly exceeds the norm. In Table 2, YS, UTS, EB_{2in} and EB_{8in} refers to the yield strength, ultimate tensile strength, and elongation at break as determined from the 2 in gauge length specimen and 8 in gauge length specimen, respectively. When validating a model of a tank car against impact test data, it is important that the material behaviors used in the FE model represent the actual behavior of the TC128 steel in the tested tank car to allow for an accurate comparison between the tested car and modeled car.

Table 2. Minimum Properties for TC128 [1]

Property	Value
YS	50,000 psi
UTS	81,000 psi
EB_{2in}	22%
EB_{8in}	16%

1.2 Objectives

The objectives of this research were: (1) present technical results from calibrating plastic material behaviors for TC128 steel using inverse (i.e., iterative) and regression approaches, (2) compare the resulting stress-strain behaviors resulting from the two approaches, and (3) discuss lessons learned from characterizing TC128 steel for use in FE analysis of tank cars.

1.3 Overall Approach

FRA conducted a series of shell impact tests on various tank car designs (see Table 1). The research team created pre-test FE models used during test planning to estimate the impact speed for many of these tests. After each test, researchers validated the FE model using the actual test conditions and steel properties. The validated FE model can then be used to analyze the performance of the tank car under different accident conditions to inform performance requirements.

This report focuses on the calibration of TC128 material models used as inputs in the pre- and post-test FE models of the shell impact test. The FE models of the shell impact test require accurate representation of the plastic hardening and ductile fracture behavior of TC128.[2] This report presents two approaches to calibrating the plastic stress-strain response of a given specimen of TC128 steel using the results from standardized tensile tests. One calibration approach was developed for use with test data that include measurements of the full stress-strain response, and the other calibration approach uses regression to estimate the plastic stress-strain response when only a summary of material properties is available from tensile testing.

1.4 Scope

This report includes a discussion on developing and executing some of the FE models used in the tank car research program (namely modeling tensile tests of TC128), outlines tensile test results, discusses the execution of the tensile tests, and summarizes the overall results of the tests. It includes discussion of calibrating a set of regression equations based on tensile tests of TC128 steel from several tank car tests, using those regression equations to estimate the stress-strain response curves for two additional examples of TC128 steel. This report also includes the equations and processes used to adapt tensile test measurements into input data for specific FE software that describes the plasticity responses of TC128 steel samples.

While this report refers to previously performed shell impact tests on different tank cars, there is no comparison of shell impact results from different tests within the scope of this report. This research was focused on calibrating the plastic stress-strain response of the TC128 material model. While the TC128 material models developed using the techniques and tensile test results described in this research are implemented into simulations of full-scale shell impact tests, the results of those shell impact simulations are absent in this report. Research into the puncture resistance of tank cars is ongoing, and further advancements in plasticity and fracture modeling will likely be considered in future work.

1.5 Organization of the Report

Section 2 describes the approach used to calibrate several TC128 steel σ_t versus ε^{pl} responses from previously tested tank cars. Section 3 describes a process to develop sets of regression equations using data from tank car Test 6 through Test 9 to estimate the σ_t versus ε^{pl} response of TC128 steel when only the YS, UTS, and EB_{2in} or EB_{8in} measurements from a tensile test are available. Section 4 contains a comparison of the σ_t versus ε^{pl} responses obtained from the TC128 steel in the Test 11 and Test 14 tank cars using both the calibration process described in Section 2 and the regression estimation from Section 3. Section 4 also includes discussion of

---

[2] Calibrating ductile fracture behavior of TC128 steel was discussed in a previous companion report [2].

some recent differences observed in “as-built” TC128 steel properties compared to the minimum specification requirements. Section 5 includes a summary of the report and contains concluding remarks.

Appendix A describes the process of deriving the regression relationships discussed in Section 3.

2. Calibrating True Stress-strain Behaviors using Full Range Tensile Test Data

Previous simulations of tank car impact tests included the ability to simulate both permanent (i.e., plastic) deformation and progressive failure, leading to element deletion and tank puncture. A previous study conducted by the Volpe Center under FRA's sponsorship focused on the fracture behaviors needed to simulate puncture of TC128 steel [2]. The present work is focused on the plastic stress-strain behavior that is used in conjunction with the fracture behaviors to simulate TC128 steel.

2.1 Introduction to Representing Plasticity in FE Models

The material input behaviors for TC128 steel used by researchers have specifically been developed for use in the Abaqus/Explicit FE software [17]. Abaqus/Explicit is a commercially available, general purpose explicit FE solver. The team used this software throughout the FRA-sponsored tank car puncture modeling program because of its ability to support several modeling techniques required to accurately represent the behavior observed in the different tank car tests. Those modeling techniques include non-linear material behavior for steels, material failure and fracture behaviors, general contact, and the ability to model the liquid (i.e., innage) and gas (i.e., outage) within each tank car.

The focus of this report is on the development of material input behaviors that describe the true plastic stress-strain response of TC128 steel. In the modeling approach that the team typically used for tank car impact simulations, there are four material "keywords" in the Abaqus software that are used to describe the properties of TC128 steel. Table 3 summarizes the keywords along with the units used in the FE models.

Table 3. Keywords Used to Describe TC128 Behaviors in FE Models

Keyword	Description
**Density*	Defines a material density in terms of mass per unit volume
**Elastic*	Defines a linear elastic modulus (E) in terms of force per unit area
**Plastic, Hardening=Isotropic*	Defines isotropic plastic hardening in terms of true stress (σ_t) and true plastic strain (ε^{pl})
**Damage Initiation, Criterion=Ductile*	Defines a fracture locus for ductile metals in terms of ε^{pl} and stress triaxiality (η)
**Damage Evolution, Type=Energy*	Defines an energy-based damage progression controlling element stiffness degradation and eventual element removal in terms of fracture energy per unit area

Figure 3 shows an exemplar nominal (i.e., engineering) stress (σ_{nom}) versus nominal strain (ε_{nom}) output from an FE model of a tensile coupon of TC128 steel with annotations showing regions affected by the various material keywords presented in Table 3. This diagram shows that the **Elastic* keyword affects only a small portion of the total σ_{nom} versus ε_{nom} response. The **Plastic* keyword determines most of the σ_{nom} versus ε_{nom} response of the coupon and therefore greatly affects the fracture toughness (i.e., area under the curve). **Damage Initiation* acts as a trigger when elements reach a threshold ε^{pl} value for a given stress triaxiality, η. After damage is triggered, **Damage Evolution* determines the rate at which the stiffness of a given element is degraded until its stiffness reaches zero and the element is removed from the simulation. Fracture is completed once all the elements across a cross-section of the coupon are removed; at that point (i.e., elongation at break) stress returns to zero.

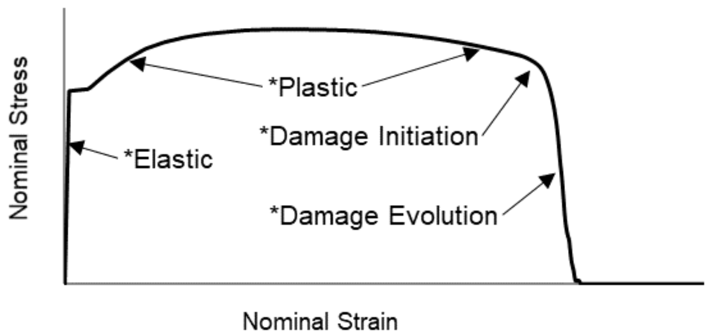

Figure 3. Annotated Nominal Stress-Strain FE Model Result for TC128 Steel

This report describes the material inputs (i.e., keywords) in the format for Abaqus/Explicit, but analogous material inputs have been developed [4] for other commercial explicit FE software including LS-DYNA [18] and with the same overall approach. Density, elastic, and plastic material properties can be specified in LS-DYNA in a material keyword such as **MAT_PIECWISE_LINEAR_PLASTICITY (024)*. Damage initiation and evolution can be specified in a material damage keyword such as **MAT_ADD_DAMAGE_DIEM* or **MAT_ADD_DAMAGE_GISSMO*.

The following sections focus on the development of the **Plastic* response of TC128 using two different approaches. Section 2 describes the process of calibrating the **Plastic* response when tensile test data are available for the full range of stresses and strains measured during a tensile test up to the point of coupon fracture. Section 3 describes the development and application of a set of regression equations to estimate the shape of the **Plastic* response for TC128 steel when only the YS, UTS, and EB_{2in} for a 2-inch gauge length or EB_{8in} for an 8-inch gauge length specimen are available from tensile testing.

2.2 Plastic Hardening of TC128

In previous tank car impact simulations using TC128 steel the plastic portion of the stress-strain response was defined as a piecewise linear function of ε^{pl} and σ_t. Generally, tensile tests report σ_{nom} and ε_{nom}. σ_{nom} is the tensile force applied to the specimen divided by its initial cross-sectional area in the gauge section. ε_{nom} is the change in length of the gauge section divided by its initial length. Even if the measurements made during a tensile test include values for ε_{nom} and σ_{nom} up to the point of break, these measurements must be transformed into σ_t and ε^{pl} for the FE solver. The relationship between σ_{nom} and σ_t is shown in Equation 1. The relationship between ε_{nom} and ε^{pl} is shown in Equation 2.

Equation 1. Calculation of σ_t from σ_{nom}

$$\sigma_t = \sigma_{nom} \cdot (1 + \varepsilon_{nom})$$

Equation 2. Calculation of ε^{pl} from ε_{nom}

$$\varepsilon^{pl} = ln(1 + \varepsilon_{nom}) - \frac{\sigma_t}{E}$$

A schematic illustration of a typical σ_{nom} versus ε_{nom} curve for TC128 steel is shown in Figure 4, with several areas of interest highlighted. Typical TC128 steel responses include an initial area of plasticity referred to as a Lüders band in which the stress remains relatively constant over some range of plastic strains. Lüders bands are common in carbon manganese steels, such as TC128, due to the presence of the interstitial atoms inhibiting the dislocation motion [19]. The stress-strain curve can be separated into three segments: the linear elastic region, the Lüders band at the onset of plasticity, and the portion of the plastic response that extends through the UTS up to the specimen breaking. Ideally, the modeled plasticity behavior should be capable of representing the response from the yield strain at the start of the Lüders band up to the growth and coalescence of microscopic voids, finally resulting in break.

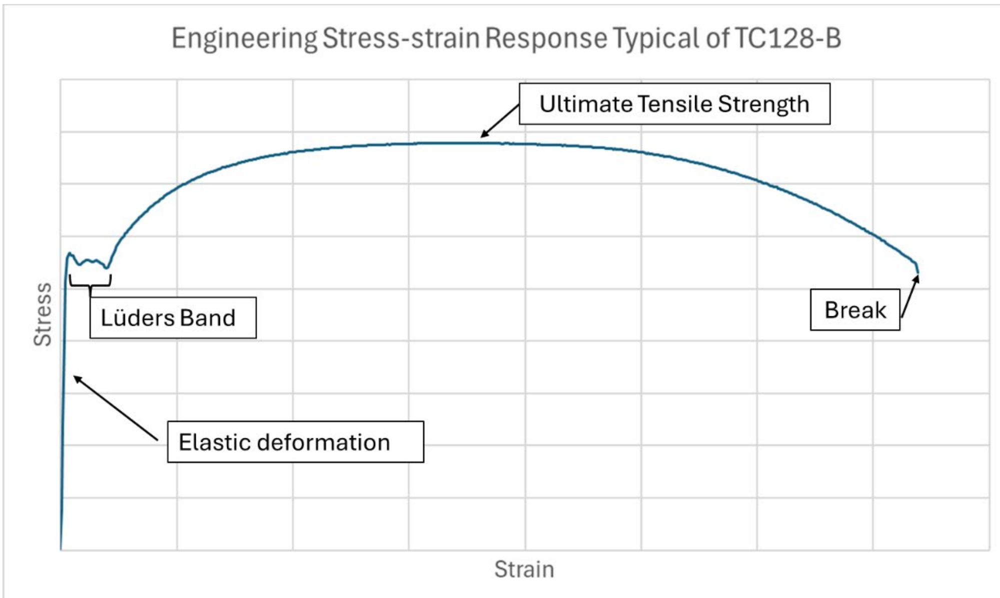

Figure 4. Annotated Nominal Stress-Strain Test Result for TC128 Steel

When the σ_{nom} versus ε_{nom} data are measured for the full tensile test and available to modelers, the process of calibrating σ_t versus ε^{pl} responses required by the simulation software is straightforward up to the onset of necking. If the σ_{nom} versus ε_{nom} response shown in Figure 4 is transformed by Equation 1 and Equation 2 the resulting σ_t versus ε^{pl} response is shown in Figure 5. An annotation on this figure shows the transformed point corresponding to the UTS in Figure 4. This point indicates the onset of necking behavior as the UTS occurred at the maximum force measured during the tensile test.

Necking dominates the σ_{nom} versus ε_{nom} response of the tensile coupon characteristic after the maximum force is achieved. The true stress-plastic strain relationship must be extrapolated for strains beyond the strain corresponding to maximum force measured during a tensile test.

If full-range stress-strain data were measured during a tensile test, the extrapolated portion of the σ_t versus ε^{pl} response could be iteratively determined through simulation of a tensile test. This iterative approach is referred to as the inverse method. The σ_{nom} versus ε_{nom} response can be obtained as output from a simulated tensile test and compared with the measure data from the tensile test. If the output from the simulation is not in acceptable agreement with the test, the points defined using **Plastic* can be adjusted in an iterative approach.

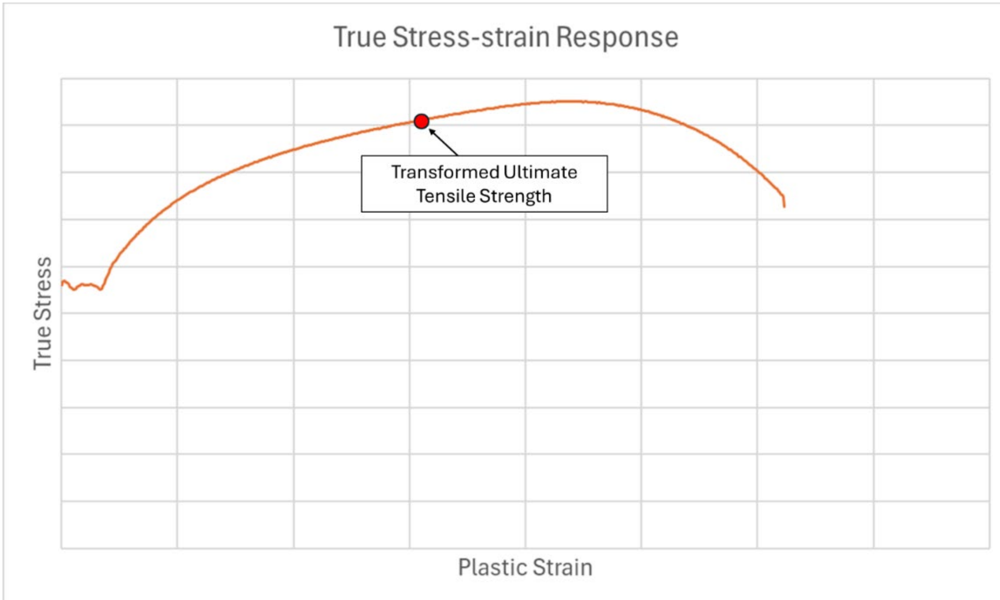

Figure 5. Plastic True Stress-Strain Test Result for TC128 Steel

2.3 Linear Extrapolation of Plastic Hardening

An example of the discrete points used to define **Plastic* in an FE model is shown in Figure 6, overlaid on the σ_t versus ε^{pl} curve shown in Figure 5. In this figure an additional point is defined under **Plastic* at a high value of plastic strain to linearly extrapolate the true plastic stress-strain response beyond the point of plastic instability or necking.

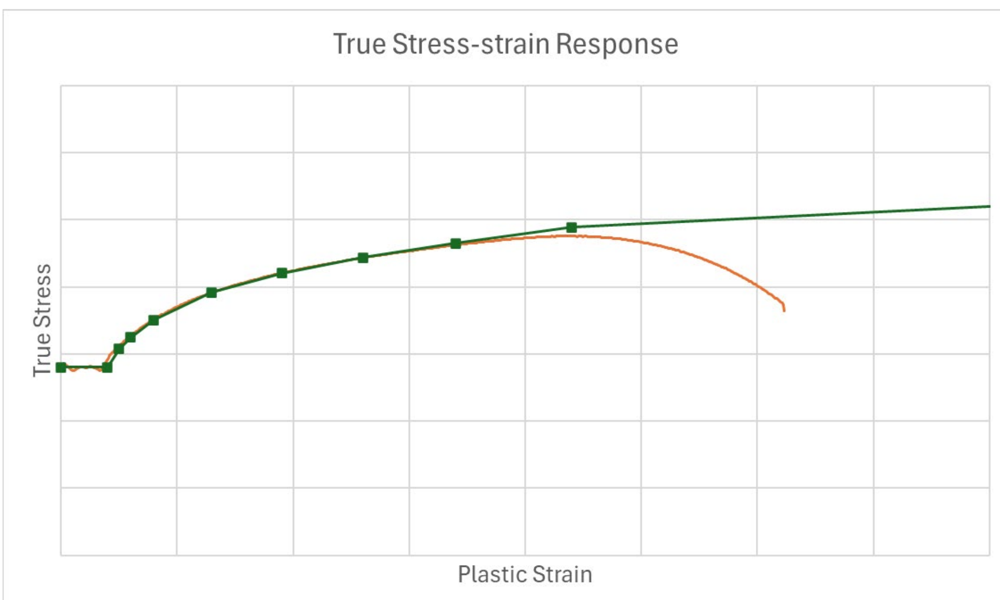

Figure 6. Plastic True Stress-Strain Response and Input from FE Model Input (with Linear Extrapolation) for TC128 Steel

Researchers have used multiple approaches to calibrating the points used to define **Plastic* in an FE model against tensile test data from TC128 steel. The approach used in progressive tank car impact tests (see Table 1) has evolved as modelers have encountered a variety of TC128 responses from different specific tank cars and developed increasing confidence in the modeling techniques used to simulate a tank car impact response.

The team's model for the TC128 steel in the Test 3 [5] tank car was based on the TC128 steel material model developed by Kirkpatrick for earlier tank car tests [4]. The Test 5 simulation used a simple bilinear response for elastic-plastic behavior, with the plastic response based on the minimum values of strength and ductility for TC128 steel [7]. Samples of TC128 steel were not excised from the tank cars used in Tests 3 or 5 for tensile testing.

Post-impact tensile testing of the TC128 from the respective tank cars were conducted for both Test 6 [8] and Test 7 [9]. The laboratory contractor measured the full range of stress-strain responses up to break for both examples of TC128 steel. The post-test simulations for Test 6 and Test 7 used *Plastic* behaviors calibrated against this actual tensile test data from each tank car's TC128 steel. The process of calibrating the *Plastic* response using test data for Tests 6 and 7 consisted of manually fitting σ_t and ε^{pl} points to the test data, simulating the coupon test, and adjusting the points to obtain reasonable agreement with the tensile test measurements.

Test 6's σ_t versus ε^{pl} response was calibrated using the inverse method with linear extrapolation. For Test 6, the σ_{nom} versus ε_{nom} data from the tensile test was first transformed into σ_t and ε^{pl} according to Equation 1 and Equation 2. The values defined in *Plastic* for σ_t and ε^{pl} were manually fit to the Lüders band portion of the transformed test data. An additional data point was added at a ε^{pl} of 1.0 to linearly extrapolate the hardening curve beyond the measured tensile data. Based on iterative simulations of tensile tests, the stresses used in *Plastic* beyond the end of the Lüders band were iteratively adjusted to obtain reasonable agreement with simulation of the tensile test. The points used to define the *Plastic* input for Test 6 TC128 steel are shown alongside the transformed stress-strain response from the coupon test used to calibrate the material model in Figure 7.

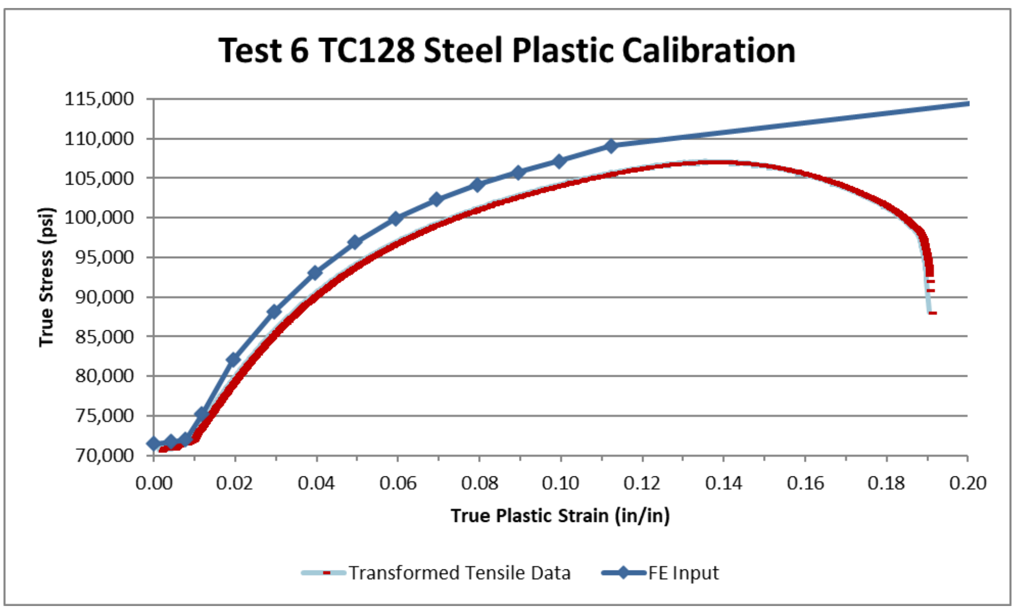

Figure 7. Test 6 True Plastic Stress-Strain FE Input and Test Result

Like Test 6, the σ_{nom} versus ε_{nom} data for Test 7's TC128 was first transformed into σ_t and ε^{pl} according to Equation 1 and Equation 2. Data points for σ_t and ε^{pl} were manually fit through the Lüders band. Discrete points were fit to the portion of the transformed plastic data from the tensile test between the upper limit of the Lüders band and maximum true stress, which occurred at a ε^{pl} of 0.216 for the sample used in the calibration. Using the inverse method, values for true stress were manually fit for ε^{pl} values of 0.17, 0.22, and 1.22.

Figure 8 shows the transformed tensile test data alongside the points used to define the **Plastic* behavior in the FE model. The points that were manually fit are indicated using hollow square points and the points that were directly transformed from the test data are shown as filled circles.

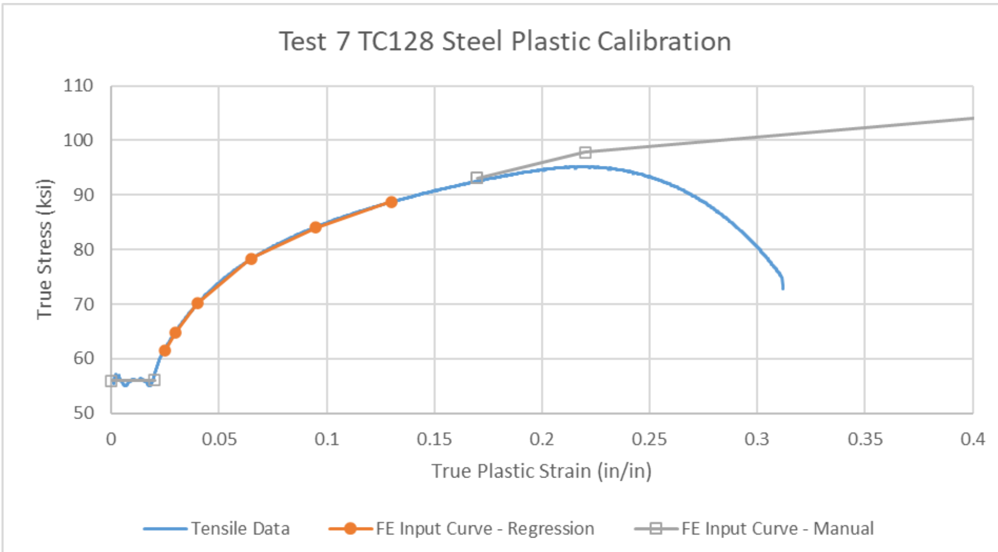

Figure 8. Test 7 True Plastic Stress-Strain FE Input and Test Result

2.4 Swift (Power) Law Plastic Hardening

Beginning with Test 8 [10], researchers began to use a Swift (power) Law model [20] of plastic hardening to develop the σ_t versus ε^{pl} relationship for TC128 steel after the Lüders band. The Swift model assumes a power law relationship between σ_t and ε^{pl}. The Swift Law is shown in Equation 3.

Equation 3. Swift (Power) Law for Plastic Hardening

$$\sigma_t^{Swift}(\varepsilon^{pl}) = A \cdot (\varepsilon_0 + \varepsilon^{pl})^n$$

Test 8 tensile testing was performed using several coupon geometries. Researchers wanted to examine whether using different coupon geometries, as allowed by the tensile testing standard ASTM E8 [21], would produce a different calibration for the **Damage Initiation* response defined as a model input [2]. The 2-in gauge length SRB specimens were used to calibrate the TC128 behavior incorporated into the Test 8 tank car model [10]. Like previous tests, the σ_t and ε^{pl} points were manually fit to the transformed test data in the Lüders band. Data points for σ_t and ε^{pl} were also manually fit between the end of the Lüders band and the UTS of the material. Beyond UTS, the Swift expression was used to estimate the isotropic hardening of the TC128 steel up to a strain of 1 in/in. The Swift expression was fit to a window of the transformed test data using a least-squares regression. The values of *A* and *n* were iteratively determined using the inverse method by adjusting the length of the fit window until the post-necking output from the coupon simulation agreed with the test data.

Figure 9, which comes from the Test 8 report [10], shows the transformed σ_t versus ε^{pl} response from the tensile coupon used to calibrate the **Plastic* material input and the portion of the transformed curve used to calculate the *A* and *n* used in Equation 3. The data points calculated using Equation 3 are shown as discrete red circles. The FE output from a simulation of the tensile test was also transformed into σ_t and ε^{pl} and is shown as a black line. The test stress-strain curve (887HHH) was transformed into σ_t and ε^{pl} and is shown as a black line for comparison.

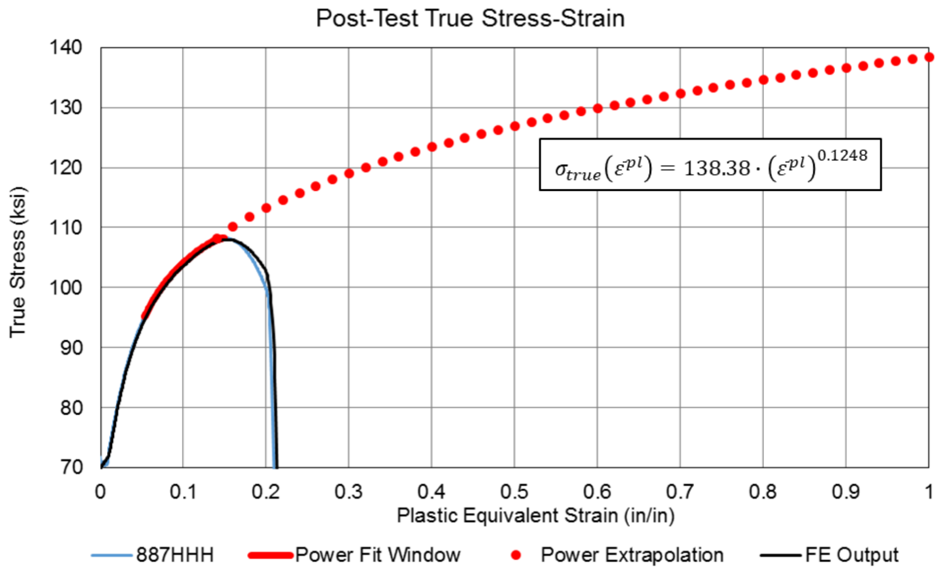

Figure 9. Test 8 True Plastic Stress-Strain FE Input, FE Output, and Test Data

Like Test 8, post-impact tensile testing of TC128 steel from the Test 9 tank car was performed using different coupon geometries. The Test 9 TC128 steel **Plastic* behavior was calibrated the same way as the Test 8 data. For Test 9, a 1.4-in gauge length SRB was used for tensile testing that was used to calibrate the **Plastic* behavior. The resulting σ_t versus ε^{pl} response for Test 9 is shown in Figure 10.

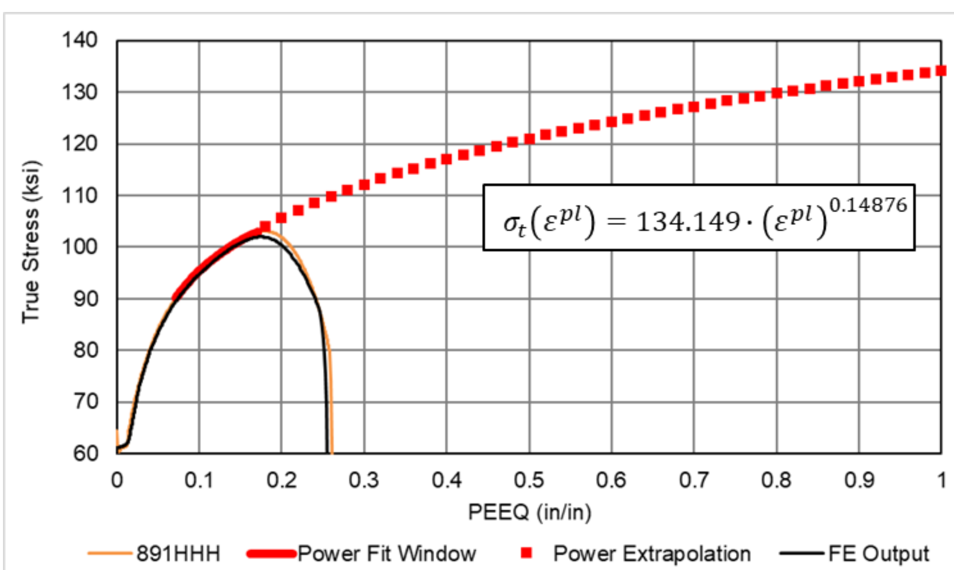

Figure 10. Test 9 True Plastic Stress-Strain FE Input, FE Output, and Test Data

For Test 11 [13] the TC128 steel was of similar strength and ductility to the TC128 from Test 9. The Test 9 **Plastic* input calibrated using SRB specimens was scaled by a factor of 1.04 to calibrate the Test 11 **Plastic* input. This scaling factor was determined through iteratively simulating a tensile test and comparing the model outputs with the tensile test measurements.

The mechanical properties of the TC128 steel taken from the Test 12 [14] and Test 13 [15] tank cars were found to be similar to the mechanical properties of the Test 11 TC128 steel. The Test 11 material calibration was also used for the simulations of Tests 12 and 13.

2.5 Mixed Swift-Voce Law Plastic Hardening

Paredes et al. (2018) applied a Mixed Swift-Voce Law hardening expression to extrapolate true stress at high strains for TC128 steel [22]. The Mixed Swift-Voce Law is a conjunction of the Swift (power) Law [20] and the Voce (exponential/saturation) Law [23], both of which describe plastic hardening. The Mixed Swift-Voce Law is a function of ε^{pl} and is formed by combining the Swift term (σ_t^{Swift}) with the Voce term (σ_t^{Voce}) using a weighting factor (α) as shown in Equation 4. The Swift term, σ_t^{Swift} remains as shown in Equation 3.

Equation 4. Voce (Exponential/Saturation), and Mixed Swift-Voce Laws for Plastic Hardening

$$\sigma_t^{Voce}(\varepsilon^{pl}) = K_0 + Q \cdot (1 - e^{-\beta\varepsilon^{pl}})$$

$$\sigma_t^{Mixed} = \alpha \cdot \sigma_t^{Swift} + (1 - \alpha)\sigma_t^{Voce}$$

Researchers used the Mixed Swift-Voce Law to calibrate the **Plastic* inputs for the Test 14 TC128 steel [16]. The Test 14 tensile test was performed using 2-inch DB coupon geometry [16]. Like the other TC128 calibrations, the first step in the process was to transform the σ_{nom} versus ε_{nom} into the σ_t versus ε^{pl} behavior. The σ_t values in the Lüders band were manually defined in the **Plastic* behavior. The Swift-Voce constants were calibrated using the transformed σ_t versus ε^{pl} data from a tensile test and performing a least squares regression fit on the Swift and Voce equations. The Swift and Voce expressions were independently fit on the transformed test data from a value of ε^{pl} close to the end of Lüders band to the ε^{pl} at maximum force because the plastic behavior of the coupon is not dominated by necking for that range of strains. After the constants for the Swift and Voce expressions (A, n, ε_0, K_0, Q, and β) were independently determined by least-squares regression, an FE model of the uniaxial tensile test was iteratively executed while varying α until the coupon model captured the post-necking behavior observed during the test. The resulting σ_t versus ε^{pl} behavior input to **Plastic* for Test 14 TC128 steel is shown in Figure 11.

From inspection of Equation 4, if α is equal to 1.0 the mixed Swift-Voce Law reduces to the Swift (power) Law. This allows for a meaningful comparison between TC128 steel material models represented using the Swift Law or the mixed Swift-Voce Law, as the coefficients *A* and *n* are common to both the pure Swift and the mixed Swift-Voce law. Table 4 summarizes the Swift-Voce coefficients developed for Test 8, Test 9, and Tests 11-14 TC128 steel. The Swift-Voce coefficients developed by Paredes et al. [22] from a modern TC128 steel tank car are also shown for comparison. It should be noted that Paredes et al. did not manually select points to capture the Lüders band.

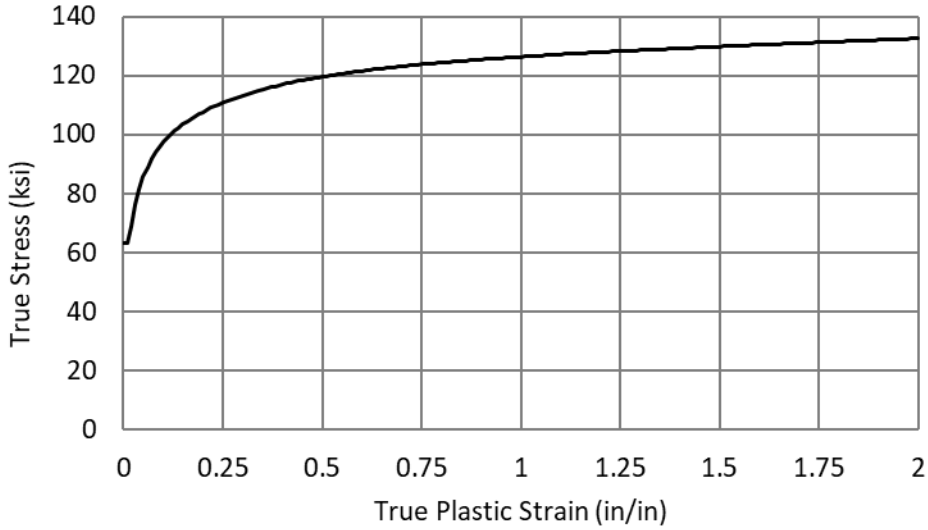

Figure 11. Test 14 True Plastic Stress-Strain FE Model Input

Table 4. Summary of Swift-Voce Parameters for TC128 steel in Tests 8-14

			A	**n**	**ε_0**	**K_0**	**Q**	**β**	**α**	**Ref**
Test	**Coupon Geometry**	**Hardening Law**	**ksi**	**-**	**-**	**ksi**	**ksi**	**-**	**-**	
8	SRB-2in	Swift	138.38	0.12484	0	0	0	0	1	[2]
8	DB-2in	Swift	133.84	0.11883	0	0	0	0	1	[2]
9	SRB-1.4in	Swift	134.15	0.14876	0	0	0	0	1	[2]
9	DB-2in	Swift	127.27	0.14753	0	0	0	0	1	[2]
11	Scaled from Test 9	Swift	139.52	0.14876	0	0	0	0	1	[13]
12	Same as Test 11	Swift	139.52	0.14876	0	0	0	0	1	[14]
13	Same as Test 11	Swift	139.52	0.14876	0	0	0	0	1	[15]
14	DB-2in	Swift-Voce	139.09	0.15355	-0.00285	80.911	250.89	0.66192	1.2	[16]
-	DB-1in	Swift-Voce	160.37	0.20000	0.005	57.06	54.22	18.5	0.6	[22]

3. Estimating True Stress-strain Behaviors Using Summarized Mechanical Properties

In Section 2 the σ_t versus ε^{pl} responses were calibrated using a variety of approaches. For all calibrations, a fundamental assumption is that the σ_{nom} versus ε_{nom} data were measured over the entire duration of the corresponding tensile test. Having the full range stress-strain data permits the discrete points used to define **Plastic* behavior to be directly matched to data points from the tensile test, or by using a regression equation and reducing the error between the test measurement and the model output.

It is not always practical to measure the full range stress-strain curve during a tensile test. For example, a material that undergoes a significant amount of elongation before break could exceed the capacity of the gauge used to measure elongation. In other cases, the gauges may be permanently damaged if the specimen fractured while the gauges were attached. Results of tensile tests are often reported as a summary table of the nominal YS and UTS as well as EB_{2in} or EB_{8in}. These are the minimum results that would be needed to determine whether the specific source of TC128 steel meets the minimum mechanical properties required by the specification. Researchers developed a second calibration procedure to estimate the σ_t versus ε^{pl} behavior to define **Plastic* when only the summarized mechanical properties are available from a tensile test.

The summarized mechanical properties of TC128 steel obtained through tensile testing of specimens from Tests 8-14 are shown in Table 5. In general, the reported values are averages obtained from tensile testing of multiple specimens of the same source of TC128. This table also includes the TC128 steel that was characterized by Paredes, et al. [22].

Table 5. Summary of YS, UTS, and EB for TC128 steel in Tests 8-14

		YS	UTS	EB	Ref.
Test	**Coupon Geometry**	**ksi**	**ksi**	%	**-**
8	SRB-2in	70	94	25	[2]
8	DB-2in	69	92	29	[2]
9	SRB-1.4in	60	86	32	[2]
9	DB-2in	57	83	34	[2]
11	SRB-2in	64.9	88.8	31.5	[13]
12	DB-2in	60.2	86.2	37.5	[14]
13	DB-2in	63.2	88.4	29.3	[15]
14	DB-2in	61.9	87.9	29.0	[16]
-	DB-1in	62.2	92.5	N/R[3]	[22]

[3] Not reported

3.1 Approach to Developing Regression Equations

In the absence of full range stress-strain data from a uniaxial tensile test, the shape of the true stress-strain curve was assumed to have a similar shape to data measured from previous tests of TC128 steel. Stress-strain curve data for TC128 steel taken from the tank cars used in Tests 6 [8], 7 [9], 8 [10], and 9 [11] were used to empirically derive equations to model the true stress-strain behavior of TC128 steel given the Young's Modulus (E), YS, UTS, and $EB2_{in}$ or EB_{8in} of a sample.

Four different tensile coupon geometries were used to test the TC128 steel specimens obtained from the tank cars used in Tests 6 through 9. For all specimens the σ_{nom} versus ε_{nom} curve was measured for as much of the test as practical, ideally up to the point of specimen break. For Tests 6 and 7, a single coupon geometry was used to characterize each tank car's material. For Tests 8 and 9 multiple coupon geometries were used to characterize each tank car's TC128 steel. Multiple coupons were used to study the effects of coupon geometry on the calibration process, as described in a previous report [11]. The three geometries used for tensile testing were a 2-inch gauge length SRB, a 2-inch gauge length DB, and an 8-inch gauge length DB. Depending on the thickness of the steel plate, ASTM E8 may allow for more than one coupon shape or size to be used [21]. The number of specimens of each geometry tested from each tank car is shown in Table 6.

Table 6. Summary of Specimen Geometries Used for Each Source of TC128 Steel

	Test 6	Test 7	Test 8	Test 9
1.4-inch SRB	0	0	0	3
2-inch SRB	6	0	3	0
2-inch DB	0	3	3	3
8-inch DB	0	0	3	3

Researchers developed two regression relationships for σ_t and ε^{pl} by considering two different subsets of the specimens shown in Table 6. The first set of regressions (Regression 2-inch) considered the 2-inch SRB and 2-inch DB coupons from Tests 6-9. The second set of relationships (Regression 8-inch) used the 8-inch DB data from Tests 8 and 9.

3.1.1 Lüders Band Portion of Plastic Response

Figure 12 shows a schematic illustration of a typical σ_{nom} versus ε_{nom} curve for TC128 steel. Several notable points that will be used in the regression calculations are illustrated. These points are the ε_{nom} at the onset of the Lüders band ($\varepsilon_{Lüders1}$), strain at the end of the Lüders band ($\varepsilon_{Lüders2}$), strain at the UTS (ε_u), the YS, and the UTS.

For each specimen *YS*, *UTS*, and *EB* were reported by the test laboratory. The lower ε_{nom} limit of the Lüders band ($\varepsilon_{Lüders1}$) corresponded to the onset of plasticity (i.e., $\varepsilon^{pl} = 0$). The value for $\varepsilon_{Lüders1}$ was calculated from the YS and E according to Equation 5. Typical values of E for TC128 steel are 2.9 – 3.0 x10^7 psi.

Equation 5. Lower Nominal Strain for Lüders Band

$$\varepsilon_{Lüders_1} = \frac{YS}{E}$$

The ε_{nom} at the upper limit of the Lüders band ($\varepsilon_{Lüders2}$) was found by examination of each σ_{nom} versus ε_{nom} response for Tests 6-9 TC128. A linear regression equation was developed to relate the value of $\varepsilon_{Lüders2}$ and the EB_{2in} or EB_{8in} of each group of specimens (i.e., 2-inch DB and SRB or 8-inch DB). The regression relationships are shown in Equation 6. Derivation of the regression relationships are described in Appendix A.

Equation 6. Regression Relationships between $\varepsilon_{Lüders2}$ and EB

$$\varepsilon_{Lüders_2} = \begin{cases} 0.0494 \cdot EB_{2in} - 0.001 & [Regression\ 2 - inch] \\ 0.0379 \cdot EB_{8in} + 0.0064 & [Regression\ 8 - inch] \end{cases}$$

The stress within the Lüders band was assumed to be constant and equal to the YS. This assumption includes two simplifications. The first is that the magnitude of the stress within the Lüders band is constant. Generally, this is not true, but the variation in stress within this band was not observed to be significant within any of the individual specimens of TC128 steel from the tank cars in Tests 6-9. Second, the YS is σ_{nom} while the desired output curve must use σ_t. From Equation 1, it is apparent that the difference between σ_{nom} and σ_t increases for increasing values of ε_{nom}. Since the value for $\varepsilon_{Lüders2}$ is relatively small in all cases, the error introduced by this assumption is also relatively small.

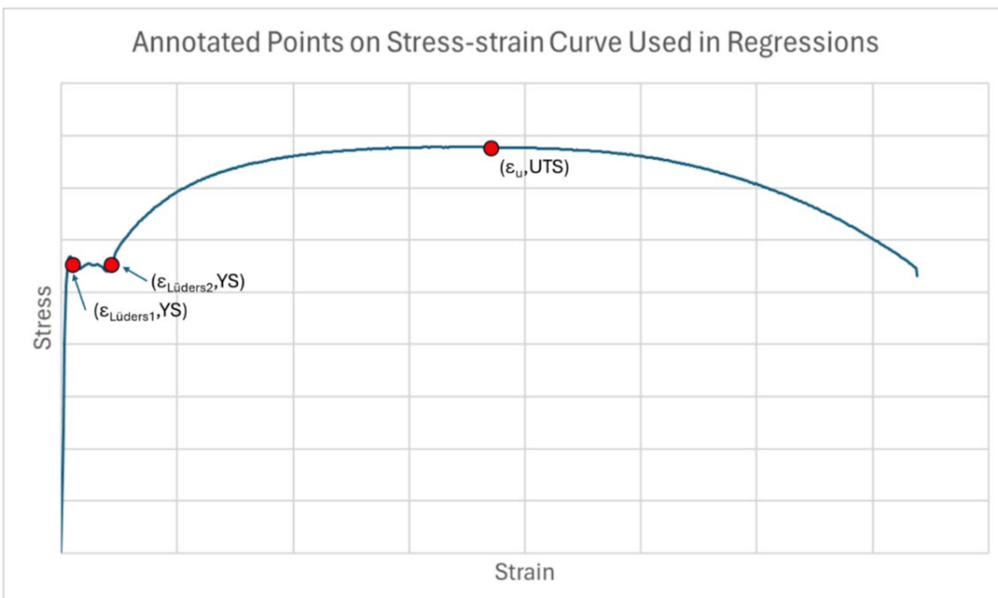

Figure 12. Annotated Points on Nominal Stress-Strain Curve Used in Regression

3.1.2 Hardening Portion of Plastic Response

Following the Lüders band, the plastic stress-strain response exhibits strain hardening behavior. In a tensile test, the maximum applied force corresponds to the UTS of the material. The ε_{nom} at UTS (ε_u) was calculated for the stress-strain data measured for each specimen of Test 6-9 TC128. The linear regression relationships between ε_u and EB_{2in} or EB_{8in}, as appropriate, were developed for the 2-inch and 8-inch gauge length specimens, as shown in Equation 7. Derivation of the regression relationships are described in Appendix A.

Equation 7. Regression Relationships between Nominal Strain at UTS and EB

$$\boldsymbol{\varepsilon_u} = \begin{cases} \mathbf{0.3121 \cdot EB_{2in} + 0.049}\ [\boldsymbol{Regression}\ \mathbf{2} - \boldsymbol{inch}] \\ \mathbf{0.4534 \cdot EB_{8in} + 0.0375}\ [\boldsymbol{Regression}\ \mathbf{8} - \boldsymbol{inch}] \end{cases}$$

Regardless of the coupon geometry regression used, the values of $\varepsilon_{Lüders1}$, $\varepsilon_{Lüders2}$ and ε_u found using Equation 5, Equation 6, and Equation 7, respectively, can be transformed into corresponding values of ε^{pl} using Equation 2, resulting in $\varepsilon^{pl}{}_{Lüders1}$, $\varepsilon^{pl}{}_{Lüders2}$, $\varepsilon^{pl}{}_{u}$, respectively.

Researchers assumed that the σ_t versus ε^{pl} response for strains greater than $\varepsilon^{pl}{}_{Lüders2}$ could be modeled using the Swift Law shown in Equation 3. The stress in the Lüders band was already considered using the procedure described in Section 3.1.1, and should not be included in the Swift Law relationship. The value of ε_0 used in Equation 3 was set to $-\varepsilon^{pl}{}_{Lüders2}$ to ensure that the Swift Law regression was only valid for strains greater than $\varepsilon^{pl}{}_{Lüders2}$.

Values for the strength coefficient (*A*) and hardening exponent (*n*) were estimated as follows. The UTS corresponds to the maximum force measured during a tensile test, which also means the slope of the nominal stress-strain response is zero at the UTS. A detailed derivation of the relationship between UTS and the exponent *n* can be found in literature [24]. From this derivation, the UTS has been shown to occur at a true strain (ε') equal to *n* [24] in materials that do not exhibit a Lüders band. Since the Swift Power Law regression is assumed to only be representative of the σ_t versus ε^{pl} curve after the Lüders band, ε^{pl} was modified by subtracting out the ε^{pl} at the end of the Lüders band, $\varepsilon^{pl}{}_{Lüders2}$. The value for *n* is thus approximated by Equation 8 for ε^{p} beyond the end of the Lüders band.

Equation 8. Approximation for Hardening Exponent, *n*

$$n = \varepsilon_U^{pl} - \varepsilon_{Lüders_2}^{pl}$$

The strength coefficient, *A*, was found by first transforming the *UTS* into σ_t using Equation 1. This value of σ_t and the value of *n* found using Equation 8 are substituted into Equation 3. Rearrangement yields Equation 9, used to approximate *A*.

Equation 9. Approximation for Strength Coefficient, *A*

$$A = \frac{UTS \cdot (1 + \varepsilon_U)}{(\varepsilon_U^{pl} - \varepsilon_{Lüders_2}^{pl})^{(\varepsilon_U^{pl} - \varepsilon_{Lüders_2}^{pl})}}$$

Discrete values for σ_t can be found by substituting values of ε^{pl} into Equation 10. The equation is valid for values of ε^{pl} greater than or equal to the onset of plasticity at $\varepsilon^{pl}{}_{Lüders1}$. Based on previous tank car puncture FE models using TC128, the σ_t versus ε^{pl} response should be defined up to a ε^{pl} of at least 1.0.

Equation 10. Piecewise Function Used to Estimate σ_t versus ε^{pl} Curve for TC128 Steel

$$\sigma_t^{Swift}(\varepsilon^{pl}) = \begin{cases} YS, \quad \varepsilon^{pl}{}_{Lüders_1} \le \varepsilon^{pl} \le \varepsilon^{pl}{}_{Lüders_2} \\ max\left[YS, A \cdot \left(\varepsilon^{pl} - \varepsilon^{pl}{}_{Lüders_2}\right)^n\right], \quad \varepsilon^{pl}{}_{Lüders_2} < \varepsilon^{pl} \end{cases}$$

4. Results and Discussion

Section 2 summarized the evolving approaches to modeling σ_t versus ε^{pl} used by researchers for TC128 steel after several FRA-sponsored tank car tests where data were measured over the full tensile test. Section 3 described a technique for estimating the σ_t versus ε^{pl} response for TC128 steel when full range data was not available for use in the calibration process. The regression relationships were developed using data from the TC128 steel obtained from the tank cars from Tests 6-9. Researchers developed σ_t versus ε^{pl} responses from two subsequent tests, Test 11 and Test 14, using test data and the iterative methods described in Section 2. As a measure of the validity of the regression method presented in Section 3, the σ_t versus ε^{pl} relationships for the Test 11 and Test 14 TC128 steels were estimated using the appropriate regression relationships and compared to the σ_t versus ε^{pl} obtained using the inverse method. This section includes discussion of several tank cars having TC128 mechanical properties below the minima of the standard that have been identified in publicly available information, illustrating the importance of understanding the "as-built" mechanical properties.

4.1 Comparing Estimated and Measured TC128 Steel Plasticity

As an evaluation on the regression technique described in Section 3, σ_t versus ε^{pl} curves for the Test 11 and Test 14 TC128 steels were calculated using only the summarized YS, UTS, and EB_{2in} data from the tensile tests even though additional data were available. The σ_t versus ε^{pl} responses produced using the regression technique were compared to the responses produced using the iterative approach as a validation of the regression technique.

The TC128 steels from Test 11 and Test 14 were both characterized by using 2-in SRB specimens. The estimated 8-inch regression was not used on the Test 11 and 14 data, as an 8-inch extensometer was not used.

Figure 13 shows an FE model of a 2-inch gauge-length SRB tensile coupon. The team used the model to compare the true plastic stress-strain responses that were calculated using the 2-inch regression methodology presented in Section 2 and Section 3. Researchers meshed the SRB model with 0.05-inch reduced integration brick elements (C3D8R), applied a 0.5-inch quasi-static displacement boundary condition to the grip end, and used 3 planes of symmetry. The 2-inch SRB model is described in detail in the Test 14 report [16]. However, this coupon model does not have ductile damage initiation or damage evolution (see Figure 3) so that only the **Plastic* behavior is compared.

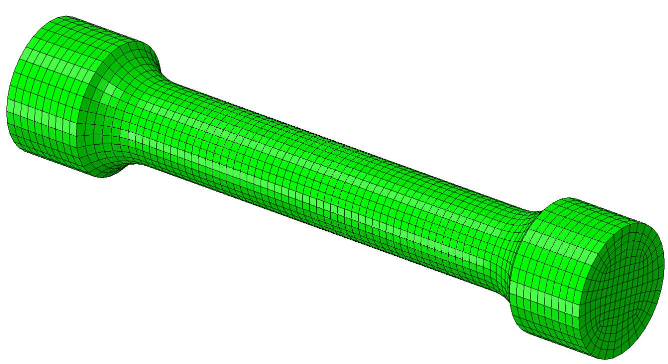

Figure 13. TC128 Smooth Round Bar 2-inch Tensile Coupon FE Model (Mirrored Across Symmetry Planes)

4.1.1 Test 11 TC128

Specimens of TC128 steel from the Test 11 tank car were tested using a 2-in SRB specimen. Two sets of regression equations were developed in Section 3: one based on data from 2-inch DB and SRB specimens and one based on 8-inch DB specimens. The 2-inch regression equations were used to estimate the Test 11 σ_t versus ε^{pl} responses. The values shown in Table 7 were the summary properties obtained from the Test 11 technical report [13] of Test 11 TC128 steel from tensile testing used in the regression equations.

Table 7. Test 11 TC128 Summary Properties Used for Regression

Property	Value	Units
E	3×10^7	psi
YS	64,900	psi
UTS	88,800	psi
EB_{2in}	31.5	%

Figure 14 shows the true plastic stress-strain FEA input (left) and nominal stress-strain FEA output (right) responses for Test 11 TC128 steel using the 2-inch regression equations and the calibrated Swift Law relationship obtained from the full stress-strain test data. The full stress-strain case is the baseline case that the 2-inch regression is trying to match while using less detailed test data. The team truncated the nominal stress-strain outputs after necking when the nominal stress dropped to a value of 1.1·YS because the model does not include ductile damage which is necessary to simulate the effects of void growth and coalescence that appear in a real tensile test.

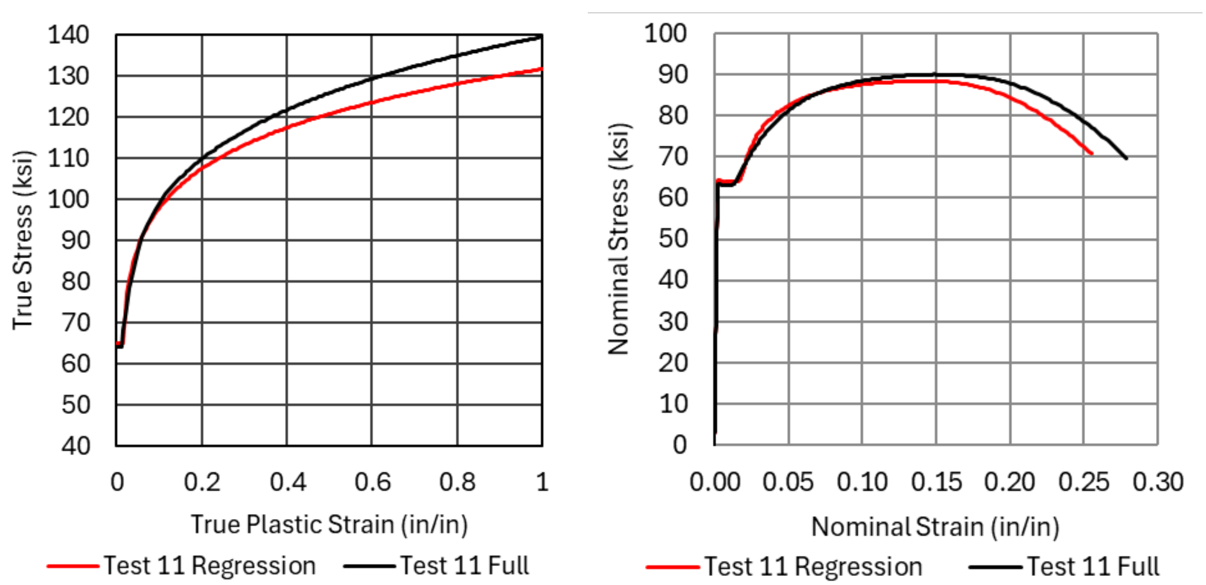

Figure 14. Test 11 TC128 True Plastic Stress-Strain FEA Inputs (left) and Nominal Stress-Strain FEA Outputs from 2-inch SRB (right)

The value of ε^{pl} at the end of the Lüders band from the 2-inch regression is in good agreement with the Test 11 calibration. The regression response is in reasonable agreement with the calibrated response for Test 11 using the full range of stress-strain test data. The agreement could be improved if the 2-inch regression had less plastic hardening immediately after the Lüders band and more plastic hardening for ε^{pl} of 0.2 in/in and greater.

4.1.2 Test 14 TC128

Specimens of TC128 steel from the Test 14 tank car were tested using a 2-in SRB specimen. The 2-inch set of regression equations was used to estimate the Test 14 σ_t versus ε^{pl} responses. The values shown in Table 8 are the summary properties obtained from the Test 14 technical report [16] from tensile testing of Test 14 TC128 steel that are used in the regression equations.

Table 8. Test 14 TC128 Summary Properties Used for Regression

Property	Value	Units
E	3×10^7	psi
YS	61,900	psi
UTS	87,900	psi
EB_{2in}	29	%

Figure 15 shows the true plastic stress-strain FEA input (left) and nominal stress-strain FEA output (right) responses for Test 14 TC128 steel using the 2-inch regression equations and the calibrated Swift-Voce relationship obtained from the full stress-strain test data. The full stress-strain case is the baseline case that the 2-inch regression is trying to match while using less detailed test data. The team truncated the nominal stress-strain outputs after necking when the nominal stress dropped to a value of 1.1·YS like in Section 4.1.1.

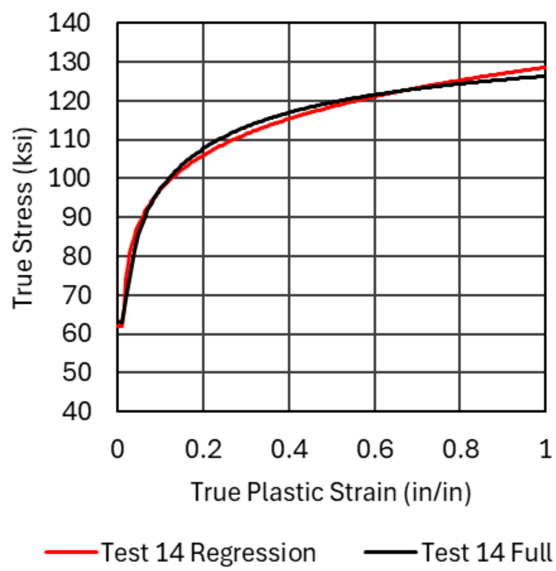

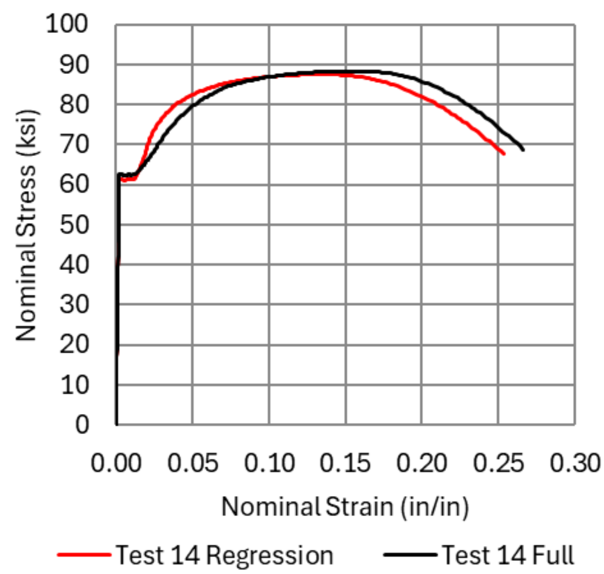

Figure 15. Test 14 TC128 True Plastic Stress-Strain FEA Inputs (left) and Nominal Stress-Strain FEA Outputs from 2-inch SRB (right)

The value of ε^{pl} at the end of the Lüders band from the 2-inch regression is in good agreement with the manually fit portion of the Test 14 Swift-Voce calibration. There is also very close agreement between the 2-inch regression and the Swift-Voce calibration for ε^{pl} between 0.1 and 0.15. There is a visible discrepancy between the 2-inch regression and the Swift-Voce calibration in the manually fit points between the end of the Lüders band and the value of ε^{pl} (0.06) where the Swift-Voce relationship was used to calibrate the stress-strain response. Similar to Test 11, the agreement could be improved if the 2-inch regression had less plastic hardening immediately after the Lüders band.

4.2 Limitation of Using Mill Material Properties

Performing tensile characterization of the specific TC128 from each tank car used in FRA's testing program has been shown to be a critical step in accurately modeling the outcome of the test. Outside of FRA's testing program, characterizing the "as-built" properties of tank car steel is rare, as they are not obtained as a routine matter because they require cutting of the tank. These properties have historically only been obtained during an investigation into the performance of a tank car following an incident, in support of modeling for a full-scale impact test, or as a research project focused on steel performance.

While modelers would ideally have tensile data prior to an impact test to allow for accurate pre-test simulations, it is generally more practical to obtain tensile specimens from the tank car after the impact test has been performed. Mill test reports from plates, also known as material test reports (MTRs), are typically provided by the steel mill to the tank car builders to demonstrate that the steel plates meets the requirements of the specification. While the data from the MTRs may be available for use in pre-test modeling, these properties have been found to differ from the "as-built" mechanical properties in a small number of cases.

Prior to Test 7 the tank car builder shared the tensile properties of the TC128 steel plate used to construct the car from the applicable MTR [9]. These results indicated that the plate met the applicable strength requirements prior to fabrication. Following Test 7, specimens of TC128 steel from the tank's shell were sent to a contractor laboratory for tensile testing. The results of the tensile testing indicated that the UTS of the steel removed from the tank car was below the minimum 81,000 psi UTS requirement of the specification for TC128 steel [1].

Following an April 24, 2019, derailment with a hazardous materials release in Fort Worth, TX, the National Transportation Safety Board (NTSB) contracted with a laboratory to perform tensile testing on specimens excised from a punctured tank car. The results of these tests indicated that the TC128 steel plate did not meet the UTS requirements of the specification [25]. NTSB contracted with a second laboratory to conduct tensile testing, with similar results. NTSB's public docket for this accident included the MTR from the steel mill for the TC128 steel plates used to construct the tank car [26]. The MTR demonstrated that the plate met the UTS requirements of TC128 steel prior to the car being fabricated.

Similarly, NTSB also contracted a laboratory to conduct post-incident tensile testing on a tank car involved in the April 26, 2024, Manuelito, NM, derailment. The results of the tensile testing indicated one tank car had YS and UTS values that were slightly below those established by the specification for TC128 [27]. NTSB's public docket for this incident did not include the MTRs, so the pre-fabrication YS and UTS cannot be included in this discussion.

These three examples of TC128 steel not meeting minimum strength in an "as-built" tank car are summarized in Table 9. As the tensile tests were generally repeated multiple times by each laboratory, the average value is provided. These average results also include testing performed in both the longitudinal and transverse directions, while the specification does not distinguish between these two directions for setting minimum properties. Shaded cells indicate average properties where one or more individual specimens were found to have values below the minimum required by the specification. In general, the values that were below the minimum values are less than 10 percent lower. No examples of "as-built" TC128 steel were identified having an EB_{2in} or EB_{8in} below the applicable minimum values. The values in the table also include the difference between the average values reported on the MTR and the average values found by tensile testing of the "as-built" car.

Table 9. Examples of Publicly Identified TC128 Steel Material with "As-built" Properties Below Specification Minima

	YS	UTS	EB_{2in}	EB_{8in}	Reference
	psi	psi	%	%	
Test 7 Car Average from MTR	62,062.5	88,854.2	-	21.6	[9]
Test 7 Car Average As-built	56,400	77,900	38.3	-	[9]
Test 7 Car Difference from MTR	-9.1%	-12.3%	-	-	-
Fort Worth Derailment UTLX 209301 Average from MTR	63,700	87,100	-	20.1	[26]
Fort Worth Derailment UTLX 209301 Average As-built	52,266.7	77,500	41.7	23.1	[25]
Fort Worth Derailment UTLX 209301 Difference from MTR	-17.9%	-11.0%	-	14.8%	-
Manuelito Derailment UTLX 954193 Average As-built	53,500	79,083.3	48.3	25	[27]
TC128 Specification	50,000 (min)	81,000-101,000	22 (min)	16 (min)	[1]

A previous FRA-sponsored study examined the mechanical properties of TC128 steel at different stages of tank car fabrication [28]. That study was conducted to better understand how the mechanical (e.g., rolling rings) and thermal (e.g., postweld heat treatment) processes used in tank car fabrication could affect the mechanical properties of the completed tank car. That study found that the postweld heat treatment stage of fabrication had the potential to both increase the TC128 steel's ductility and decrease its UTS.

The examples cited in Table 9 represent a small set of data, which cannot be extrapolated to the entire fleet of tank cars. A more comprehensive study of tank cars, similar to previous studies on the properties of tank car steel properties from retired tank cars [29] could be conducted to better understand the mechanical properties of steels in the modern tank car fleet. The previous work was published in 2008, and did not include a comparison between the "as-built" properties and the MTR values for the tank cars included in the study. An updated version of this study would better reflect the current fleet of tank cars and would allow for additional data points to be obtained relating the "as-built" mechanical properties to the properties reported on the MTRs.

4.2.1 Minimum TC128 Steel

It is preferrable to have the full stress-strain response when modeling the plastic behavior of TC128. Section 2 describes how to use a nominal stress-strain curve to define true plastic stress-strain behavior for TC128. In the absence of the full stress-strain response, Section 3 presents a methodology to estimate the true plastic stress-strain behavior for TC128 using the limited summary properties from a tensile test report. Section 4.2 discusses the limitations of using an MTR as the source of the tensile properties when estimating the true plastic stress-strain behavior of TC128. This section presents the results from using the 2-inch and 8-inch regression techniques on the minimum properties of TC128 steel set out in the material specification [1]. While theoretically possible to produce TC128 steel plate that possesses minimally acceptable values for all mechanical properties, this material should be considered an example of the hypothetical worst-case material.

Table 10 shows the minimum properties of TC128 steel used in the 2-inch and 8-inch regressions. The properties were the same for both regressions except for EB.

Table 10. Minimum TC128 Summary Properties Used for Regression

Property	Value	Units
E	3×10^7	psi
YS	50,000	psi
UTS	81,000	psi
EB_{2in}	22	%
EB_{8in}	16	%

Figure 16 shows the true plastic stress-strain FEA input (left) and nominal stress-strain FEA output (right) responses for the minimum TC128 2-inch and 8-inch regression equations from the 2-inch SRB model. No comparison is made to a calibrated response using the full stress-strain test data because the minimum TC128 properties do not correspond to actual stress-strain test data for any materials known to the researchers. The team truncated the nominal stress-strain outputs after necking when the nominal stress dropped to a value of 1.1·YS like Section 4.1.1.

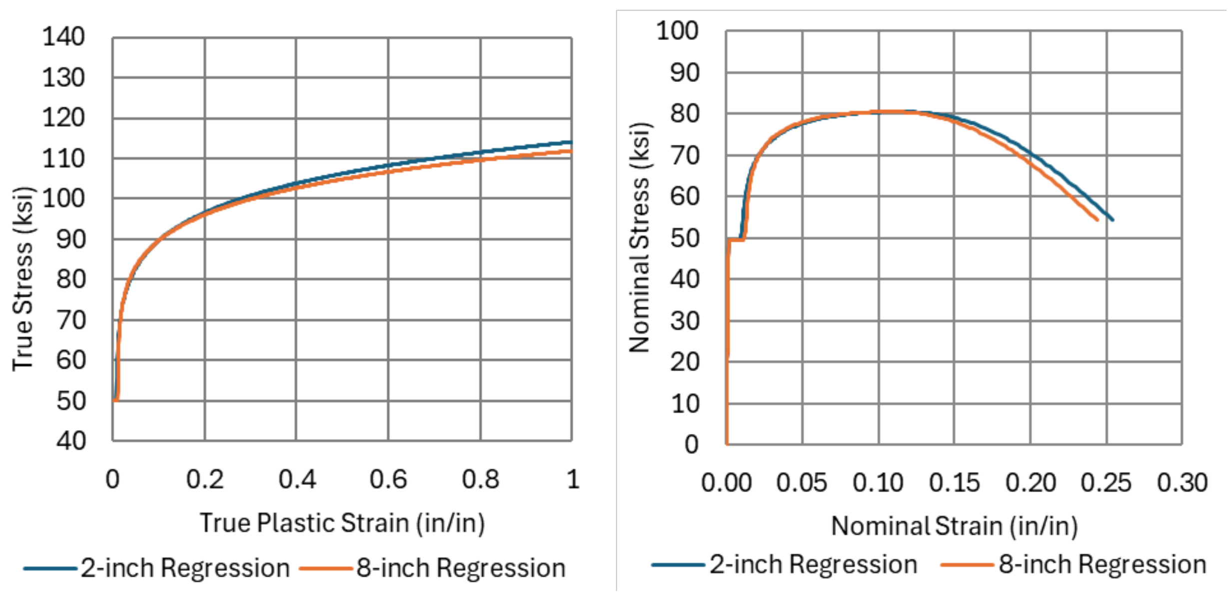

Figure 16. Minimum TC128 Comparison of 2-inch and 8-inch Regression True Plastic Stress-Strain FEA Input (Left) and Nominal Stress-Strain FEA Output from 2-inch SRB (right)

The 2-inch and 8-inch regression inputs and outputs are in good agreement with each other, and the YS and UTS values output from the 2-inch SRB model perfectly match the target minimum strength TC128 requirements. It should be noted that the 8-inch regression true plastic stress-strain curve was applied to the 2-inch SRB tensile coupon shown in Figure 13. The plastic hardening immediately after the end of the Lüders band looks unusually aggressive.

Figure 17 shows an FE model of an 8-inch gauge-length DB tensile coupon. The team used the model to compare the true plastic stress-strain responses that were calculated using the 2-inch and 8-inch regression methodology presented in Section 3. Researchers meshed the 8-inch DB model with 0.05-inch reduced integration brick elements (C3D8R) in the gauge section, applied a 1-inch quasi-static displacement boundary condition to the grip end, and used 3 planes of symmetry. This coupon model does not have ductile damage initiation or damage evolution (see Figure 3) so that only the **Plastic* behavior is compared.

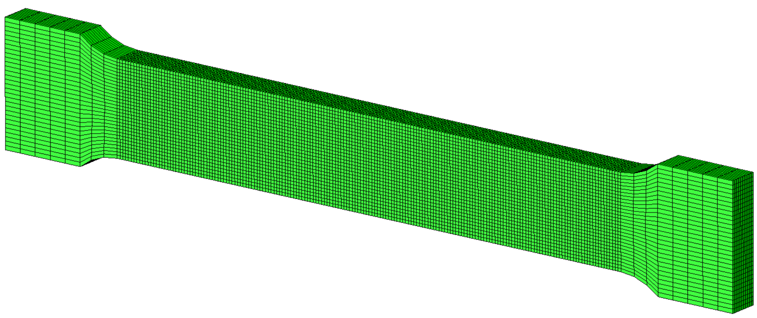

Figure 17. TC128 Dogbone 8-inch Tensile Coupon FE Model (Mirrored across Symmetry Planes)

Figure 18 shows the true plastic stress-strain FEA input (left) and nominal stress-strain FEA output (right) responses for the minimum TC128 2-inch and 8-inch regression equations from the 8-inch DB model. No comparison is made to a calibrated response using the full stress-strain test data because the minimum TC128 properties do not correspond to actual stress-strain test data. The team truncated the nominal stress-strain outputs after necking when the nominal stress dropped to a value of 1.1·YS like Section 4.1.1.

The FEA output from the 8-inch DB model is like the output from the 2-inch SRB model. The YS and UTS values output from the 8-inch DB model perfectly match the target minimum strength TC128 requirements. It should be noted that the 2-inch regression true plastic stress-strain curve was applied to the 8-inch DB model shown in Figure 17. The plastic hardening immediately after the end of the Lüders band also looks unusually aggressive, like the 2-inch SRB model. Further refinement of the regression could improve the realism of the plastic hardening curve.

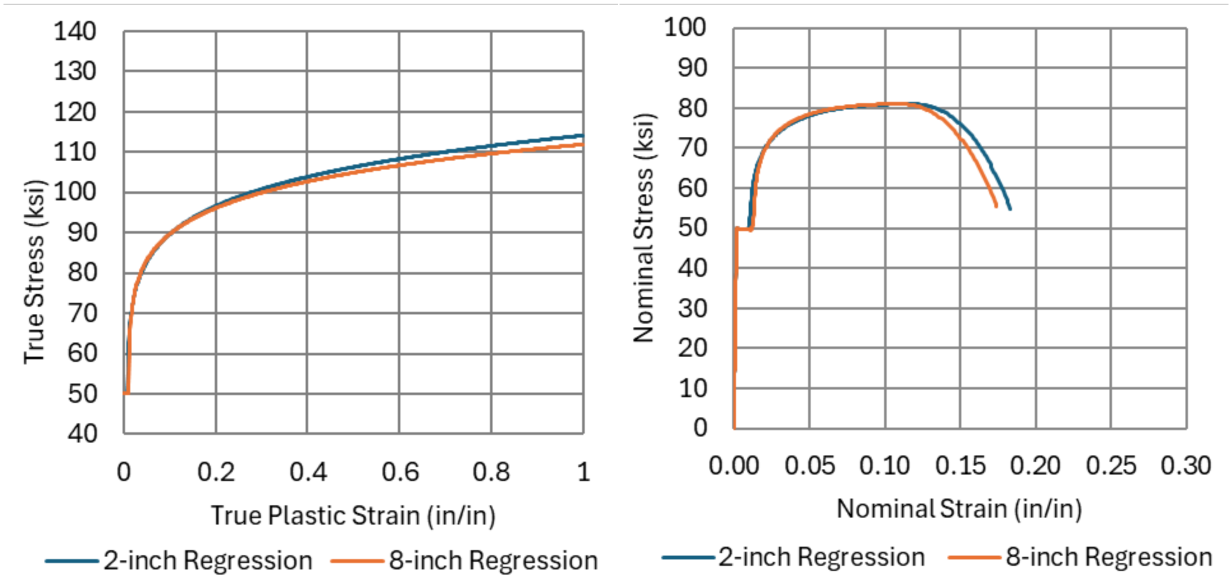

Figure 18. Minimum TC128 Comparison of 2-inch and 8-inch Regression True Plastic Stress-Strain FEA Input (Left) and Nominal Stress-Strain FEA Output from 8-inch DB (right)

5. Conclusion

This report describes two approaches to modeling the plastic stress-strain responses of TC128 steel for use in FE simulations of tank car impacts. The first approach describes the processes used by researchers when the full range of stress-strain measurements collected during a tensile test of TC128 steel are available for calibration. The process of calibrating σ_t versus ε^{pl} behavior in the format required by the Abaqus FE software has evolved from an ad hoc process of linearly extrapolating the plastic hardening after the onset of necking to using the Swift-Voce Law with the inverse method.

A second technique was described that can be used to estimate the σ_t versus ε^{pl} response when the data reported from a tensile test are limited to the YS, UTS, and EB_{2in} or EN_{8in}. Using the full range of data measured from the tensile tests of TC128 from the tank cars used in Tests 6-9, researchers developed three sets of regression equations. The first set of regression equations are based on tensile tests performed using 2-in DB specimens. The second set is based on tensile tests using both 2-in DB and 2-in SRB specimens. The third set is based on tensile tests performed using 8-in DB specimens. The set or sets of regression equations used to estimate the σ_t versus ε^{pl} behavior should correspond to the ASTM E8 standard tensile geometry used to measure the limited set of tensile properties from a TC128 specimen.

Tensile data measured for the TC128 steel from the Test 11 and Test 14 tank cars were used with both calibration methods as a means of validating the regression equations. A Swift Law relationship was used at the time of Test 11 to produce the σ_t versus ε^{pl} response used in the Test 11 post-test models, and a mixed Swift-Voce relationship was used with the Test 14 data. The regression equations for 2-in gauge-length specimens (DB and SRB) were used with the summarized YS, UTS, and EB_{2in} data measurements from the Test 11 and Test 14 TC128 steels. The estimated σ_t versus ε^{pl} responses obtained from the regression equations were found to be in reasonable agreement with the calibrated responses from the full stress-strain test data.

Additionally, the team applied the 2-inch and 8-inch regression equations using the minimum required properties of TC128 to show the resulting output from an edge case. The resulting nominal stress-strain response appears to harden too aggressively after the end of the Lüders band; however, there is no baseline case for comparison because the input values are from a hypothetical edge case.

The techniques described in this report can be employed to estimate the σ_t versus ε^{pl} response both when the full range stress-strain response is measured, or when only summary data are available. The regression equations can prove to be especially useful when tensile testing has already been performed without measuring the full stress-strain response, such as for data measured in previous research efforts. However, it is still preferrable to use the full stress-strain data to calibrate TC128's plastic behavior because the regression equations tend to overestimate plastic hardening after the end of the Lüders band. The regression technique could also be used to produce hypothetical stress-strain responses that do not correspond to a particular tensile test.

6. References

[1] Association of American Railroads (2014). AAR Manual of Standards and Recommended Practices, Section C-Part III, Specifications for Tank Cars, Specification M-1002.

[2] Eshraghi, S., & Carolan, M. (2020). Quick Calibration of Fracture Behaviors in TC128 Steel for Finite Element Modeling. U.S. Department of Transportation.

[3] Krishnamurthy, A., Trevithick, S., Carolan, M., Spangenberg, U., Wilson, N., Eshraghi, S., & Kirkpatrick, S. (2022). Review of Tank Car Side Impact Test Research and Analyses of 2007–2019. U.S. Department of Transportation.

[4] Kirkpatrick, S. (2010). Detailed Puncture Analyses of Various Tank Car Designs: Final Report - Revision 1. Applied Research Associates, Inc..

[5] Carolan, M., Jeong, D., Perlman, B., Murty, Y., Namboordri, S., Kurtz, R., Elzey, R., Ananikitpaiboon, S., Tunna, L., & Fries, R. (2013). Application of Welded Steel Sandwich Panels for Tank Car Shell Impact Protection (Report No. DOT/FRA/ORD-13/19). Federal Railroad Administration.

[6] Kirkpatrick, S., Rakoczy, P., MacNeill, R., & Anderson, A. (2015). Side Impact Test and Analyses of a DOT-111 Tank Car (Report No. DOT/FRA/ORD-15/30). Federal Railroad Administration.

[7] Rakoczy, P., & Carolan, M. (2016). Side Impact Test and Analysis of a DOT-112 Tank Car (Report No. DOT/FRA/ORD-16/38). Federal Railroad Administration.

[8] Carolan, M., & Rakoczy, P. (2019). Side Impact Test and Analysis of a DOT-105 Tank Car (Report No. DOT/FRA/ORD-19/12). Federal Railroad Administration.

[9] Rakoczy, P., Carolan, M., Gorhum, T., & Eshraghi, S. (2019). Side Impact Test and Analyses of a DOT-117 Tank Car (Report No. DOT/FRA/ORD-19/13). Federal Railroad Administration.

[10] Wilson, N., Eshraghi, S., Trevithick, S., Carolan, M., & Rakoczy, P. (2020). Side Impact Test and Analyses of a DOT-105 Tank Car – 6 X 6 Inch Indenter (Report No. DOT/FRA/ORD-20/38). Federal Railroad Administration.

[11] Eshraghi, S., Trevithick, S., Carolan, M., Rakoczy, P., & Wilson, N. (2020), Side Impact Test and Analyses of a DOT-111 (CPC-1232) Tank Car (Report No. DOT/FRA/ORD-20/43). Federal Railroad Administration.

[12] Trevithick, S., Carolan, M., Eshraghi, S., & Wilson, N. (2021). Side Impact Test and Analyses of a Legacy DOT-113 Tank Car. U.S. Department of Transportation.

[13] Wilson, N., Carolan, M., Trevithick, S., & Eshraghi, S. (2021). Side Impact Test and Analyses of a DOT-113 Surrogate Tank Car with Water. U.S. Department of Transportation.

[14] Belport, S., Carolan, M., Trevithick, S., Eshraghi, S., & Krishnamurthy, A. (2022). Side Impact Test and Analyses of a DOT-113 Surrogate Tank Car with Cryogenic Lading (Report No. DOT/FRA/ORD-22/33). Federal Railroad Administration.

[15] Eshraghi, S., Belport, S., Carolan, M., Trevithick, S., & Krishnamurthy, A. (2022). Side Impact Test and Analyses of a DOT-113C120W9 Tank Car with Cryogenic Lading. Federal Railroad Administration.

[16] DOT-105 CO2 Tank Car Report (in publication). Federal Railroad Administration.

[17] Dassault Systèmes Simulia Corp. (2023). *Abaqus 2023*.

[18] Livermore Software and Technology Corporation (LSTC) (2018). LS-DYNA Keyword User's Manual, Volume II Material Models, LS-DYNA R11. LSTC.

[19] Wang, X. G., He, B. B., Liu, C. H., Jiang, C., & Huang, M. X. (2019). Extraordinary Lüders-strain-rate in medium Mn steels. *Materialia, 6*.

[20] Swift, H. W. (1952). Plastic instability under plane stress. *Journal of the Mechanics and Physics of Solids, 1*, p. 1–18.

[21] ASTM International (2013). *ASTM E8/E8M: Standard Test Methods for Tension Testing of Metallic Materials.* American Society for Testing and Materials.

[22] Paredes, M., Sarzosa, D., Savioli, R., Wierzbicki, T., Jeong, D., & Tyrell, D. (2018). Ductile Tearing Analysis of TC128 Tank Car Steel Under Mode I Loading. *Theoretical and Applied Fracture Mechanics, 96,* pp. 658-675, 2018.

[23] Voce, E. (1948). The relationship between stress and strain for homogeneous deformations. *Journal of the Institute of Metals, 74*, p. 537–562.

[24] Hosford W. F., & Caddell, R. M. (2007). Metal Forming Mechanics and Metallurgy, Third Edition. New York: Cambridge University Press.

[25] National Transportation Safety Board (2022). Materials Laboratory Factual Report No. 19-054 - Fort Worth, Texas - April 24, 2019. National Transportation Safety Board.

[26] Mittal Steel USA Quality Department (2007). Report of Tests and Analyses, Shipment No. 803-12480.

[27] ESi Laboratory and Industrial Services (2024). Tensile Test - ASTM A370 (UTLX954193). ESi Laboratory and Industrial Services.

[28] Sullivan L., & Carolan, M. (2022). Mechanical Properties of TC-128B Steel during Multiple Stages of Tank Car Fabrication. Federal Railroad Administration.

[29] McKeighan, P. C. (2008). Mechanical Properties of Tank Car Steels Retired from the Fleet. Southwest Research Institute.

Appendix A.
Derivation of Regression Relationships

This appendix summarizes the tensile test data from Tests 6-9 used to develop the regression relationships for the ε_{nom} at the end of the Lüders band ($\varepsilon_{Lüders2}$) and the ε_{nom} corresponding to the ultimate tensile strength (ε_u). Two sets of regression relationships were developed, with each using different subsets of tensile tests. Regression 2-inch used data from all 2-inch tensile tests (e.g., both DB and SRB specimens). Regression 8-inch used data from 8-inch DB tensile tests.

For each of the regressions below the EB_{2in} or EB_{8in}, as appropriate, was calculated from the initial and final gauge length of each specimen. These values were provided in the summary reports from the applicable testing laboratory. The value of $\varepsilon_{Lüders2}$ for each specimen was obtained by visual inspection of the σ_{nom} versus ε_{nom} data measured for each specimen. The value of ε_u was also found from review of the σ_{nom} versus ε_{nom} data.

Following each table of summarized results are plots of $\varepsilon_{Lüders2}$ versus EB and ε_u versus EB. The linear regression equation for each data series has been superimposed on each plot. The linear regression equations for $\varepsilon_{Lüders2}$ versus EB were previously presented as Equation 6. The linear regression equations for ε_u versus EB were previously presented as Equation 7.

Regression 2-inch

Table A1. Summary of Properties from All 2-in DB and SRB Tensile Tests Used for Regression 2

Tank Car Test	Specimen ID	Reference	Gauge Length (in.)	Final Length (in.)	EB_{2in}	$\varepsilon_{Lüders2}$ (in/in)	ε_u (in/in)
6	R1-S1	[8]	2	2.42	21.0%	0.01128317	0.1134097
6	R1-S2	[8]	2	2.43	21.5%	0.01106416	0.1123301
6	R1-S3	[8]	2	2.44	22.0%	0.0112107	0.1264594
6	R2-S1	[8]	2	2.44	22.0%	0.0113	0.1175157
6	R2-S2	[8]	2	2.41	20.5%	0.008874217	0.1176044
6	R2-S3	[8]	2	2.42	21.0%	0.01138482	0.1224327
7	Tensile-S1	[9]	2	2.76	38.0%	0.02067933	0.1761959
7	Tensile-S2	[9]	2	2.75	37.5%	0.02010886	0.1696893
7	Tensile-S3	[9]	2	2.77	38.5%	0.02020456	0.1702702
8	887HHH	[2]	2	2.49	24.5%	0.01081929	0.1273435
8	888HHH	[2]	2	2.52	26.0%	0.009774839	0.1267792
8	889HHH	[2]	2	2.49	24.5%	0.00909912	0.118418
8	896HHH	[2]	2	2.58	29.0%	0.0111386	0.1247386
8	897HHH	[2]	2	2.58	29.0%	0.01116648	0.1263165
8	898HHH	[2]	2	2.59	29.5%	0.01127579	0.1518158
9	902HHH	[2]	2	2.65	32.5%	0.0137172	0.1518523
9	903HHH	[2]	2	2.7	35.0%	0.01411155	0.1515934
9	904HHH	[2]	2	2.66	33.0%	0.01361719	0.1528154

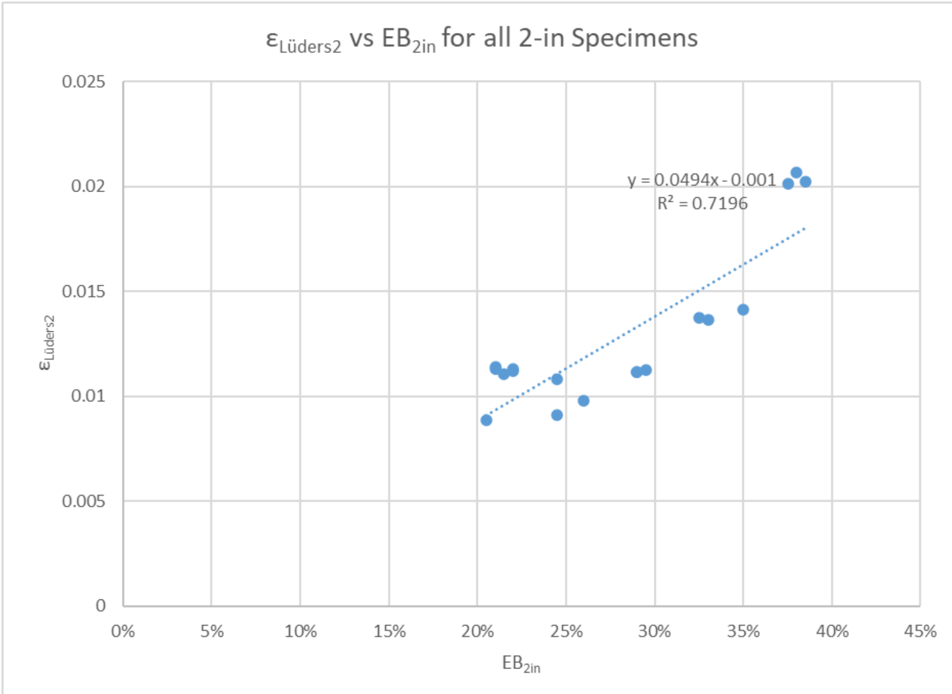

Figure A1. $\varepsilon_{Lüders2}$ vs EB_{2in} for all 2-in Specimens

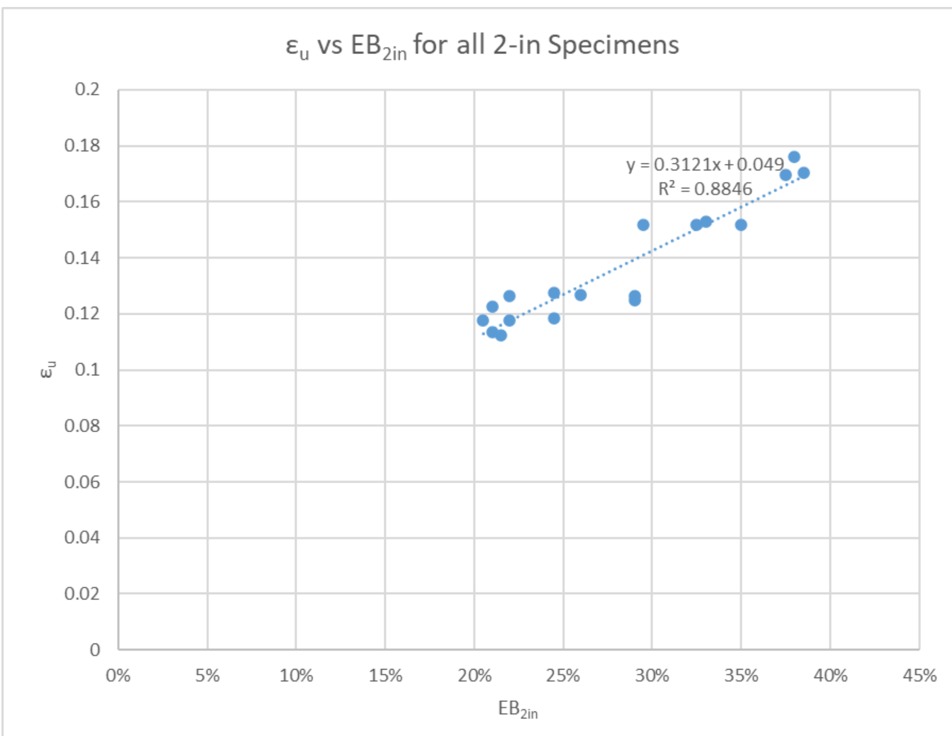

Figure A2. ε_u vs EB_{2in} for all 2-in Specimens

Regression 8-inch

Table A2. Summary of Properties from All 8-in DB Tensile Tests Used for Regression 2

Tank Car Test	Specimen ID	Reference	Gauge Length (in.)	Final Length (in.)	EB_{8in}	$\varepsilon_{Lüders2}$ (in/in)	ε_u (in/in)
8	893HHH	[2]	8	9.41	17.63%	0.01306021	0.1153502
8	894HHH	[2]	8	9.38	17.25%	0.01245992	0.1165699
8	895HHH	[2]	8	9.4	17.50%	0.0134675	0.1179075
9*	899HHH	[2]	8	9.91	23.88%	0.03792964	0.3347596
9	900HHH	[2]	8	9.81	22.63%	0.01494659	0.1416566
9	901HHH	[2]	8	9.83	22.88%	0.01501652	0.1398165

*Specimen 899HHH exhibited inconsistencies in strain measurements and was excluded from regression analysis.

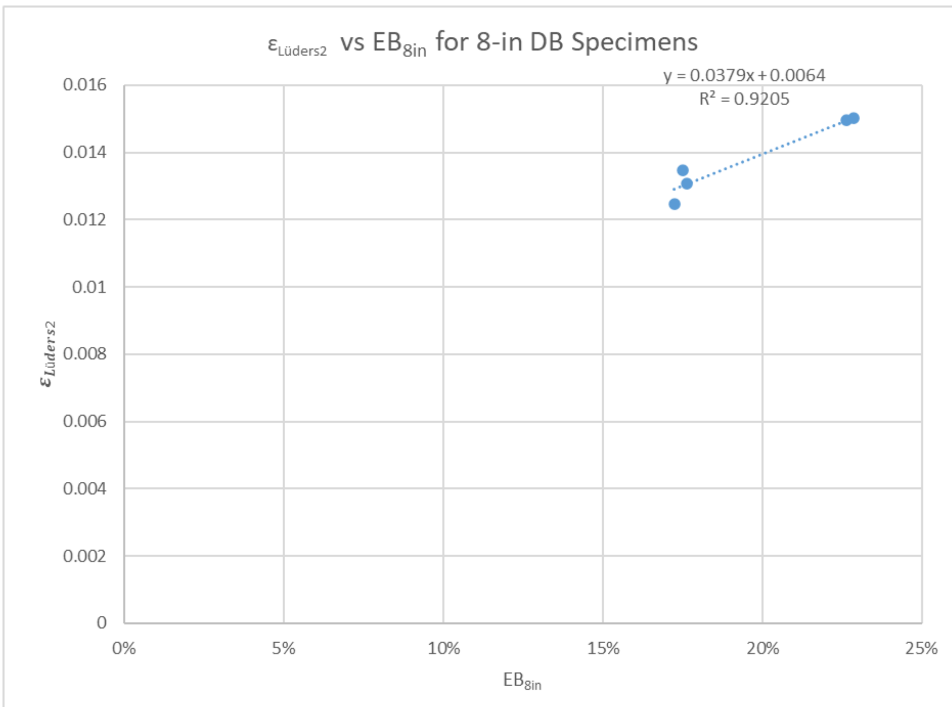

Figure A3. $\varepsilon_{Lüders2}$ vs EB8in for 8-in DB Specimens

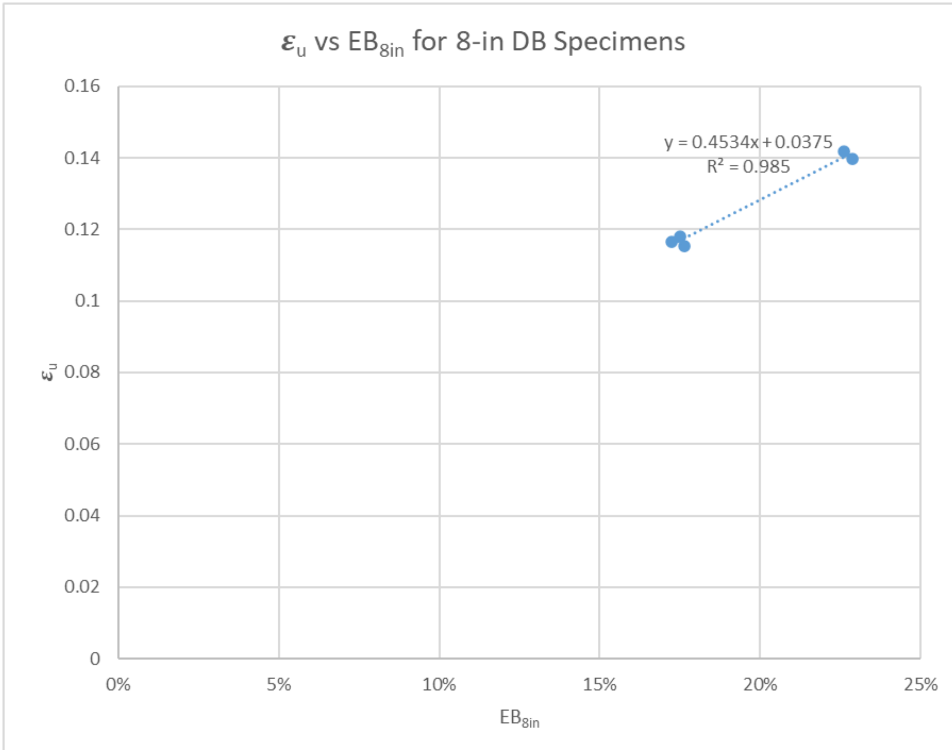

Figure A4. ε_u vs EB_{8in} for 8-in DB Specimens

Abbreviations and Acronyms

ACRONYM	DEFINITION
A	Strength coefficient
α	Weighting factor
β	Exponential term in Voce relationship
DB	Dogbone (rectangular) tensile coupon geometry
E	Young's modulus
ε'	True strain
$\varepsilon_{Lüders1}$	Nominal strain at start of Lüders band
$\varepsilon_{Lüders2}$	Nominal strain at end of Lüders band
ε_0	Offset strain
$\varepsilon^{pl}_{Lüders1}$	True plastic strain at start of Lüders band
$\varepsilon^{pl}_{Lüders2}$	True plastic strain at end of Lüders band
ε_{nom}	Nominal (engineering) strain
ε_u	Nominal strain at UTS
ε^{pl}_u	True plastic strain at UTS
ε^{pl}	True plastic strain
EB_{2in}	Elongation at break in 2-inch gauge length specimen
$EB8_{in}$	Elongation at break in 8-inch gauge length specimen
K_0	Constant in Voce equation
MTR	Mill (material) test report
NTSB	National Transportation Safety Board
n	Strain hardening exponent
Q	Hardening modulus
SRB	Smooth round bar tensile coupon geometry
σ_{nom}	Nominal (engineering) stress
σ_t	True stress
σ_t^{Mixed}	True stress from mixed Swift-Voce relationship
σ_t^{Swift}	True stress from Swift relationship
σ_t^{Voce}	True stress from Voce relationship
TTCI	Transportation Technology Center, Inc.
UTS	Ultimate tensile strength
Volpe Center	Volpe National Transportation Systems Center
YS	Yield strength